JOURNAL OF BACTERIOLOGY, Dec. 2009, p. 7383–7401 Vol. 191, No. 24
0021-9193/09/$12.00 doi:10.1128/JB.00811-09

Self-Enhanced Accumulation of FtsN at Division Sites and Roles for Other Proteins with a SPOR Domain (DamX, DedD, and RlpA) in *Escherichia coli* Cell Constriction▽†

Matthew A. Gerding,‡ Bing Liu,‡ Felipe O. Bendezú,‡§ Cynthia A. Hale, Thomas G. Bernhardt,¶ and Piet A. J. de Boer*

Department of Molecular Biology & Microbiology, School of Medicine, Case Western Reserve University, Cleveland, Ohio 44106-4960

Received 22 June 2009/Accepted 6 August 2009

Of the known essential division proteins in *Escherichia coli*, FtsN is the last to join the septal ring organelle. FtsN is a bitopic membrane protein with a small cytoplasmic portion and a large periplasmic one. The latter is thought to form an α-helical juxtamembrane region, an unstructured linker, and a C-terminal, globular, murein-binding SPOR domain. We found that the essential function of FtsN is accomplished by a surprisingly small essential domain (^{E}FtsN) of at most 35 residues that is centered about helix H2 in the periplasm. ^{E}FtsN contributed little, if any, to the accumulation of FtsN at constriction sites. However, the isolated SPOR domain (^{S}FtsN) localized sharply to these sites, while SPOR-less FtsN derivatives localized poorly. Interestingly, localization of ^{S}FtsN depended on the ability of cells to constrict and, thus, on the activity of ^{E}FtsN. This and other results suggest that, compatible with a triggering function, FtsN joins the division apparatus in a self-enhancing fashion at the time of constriction initiation and that its SPOR domain specifically recognizes some form of septal murein that is only transiently available during the constriction process. SPOR domains are widely distributed in bacteria. The isolated SPOR domains of three additional *E. coli* proteins of unknown function, DamX, DedD, and RlpA, as well as that of *Bacillus subtilis* CwlC, also accumulated sharply at constriction sites in *E. coli*, suggesting that septal targeting is a common property of SPORs. Further analyses showed that DamX and, especially, DedD are genuine division proteins that contribute significantly to the cell constriction process.

Bacterial cytokinesis is mediated by a ring-shaped apparatus. Assembly of this septal ring (SR; also called the divisome or septasome) begins at the future site of fission, well before cell constriction initiates, and it remains associated with the leading edge of the invaginating cell envelope until fission is completed. The mature ring in *Escherichia coli* is made up of at least 10 essential division proteins (FtsA, -B, -I, -K, -L, -N, -Q, -W, and -Z and ZipA), which are each needed to prevent a lethal filamentation phenotype. The first known step in assembly of the division apparatus is polymerization of FtsZ just underneath the cytoplasmic membrane. These polymers are joined by FtsA and ZipA via direct interactions with FtsZ, resulting in an intermediate ring structure (the Z ring), onto which the remaining components assemble in a specific order to form a constriction-competent complex.

In addition to the essential SR proteins, a growing number of nonessential proteins that associate with the organelle are being identified. Some of the latter are likely to serve redundant functions, while some may be required only under particular conditions (for reviews on the topic, see references 15, 19, and 25).

FtsN belongs to the essential SR proteins and is thought to be the last of this class to join the organelle before the onset of cell constriction (1, 9, 11, 57, 59). It is a type II bitopic transmembrane species of 319 residues with a small cytoplasmic domain (residues 1 to 30), a single transmembrane domain (residues 31 to 54), and a large periplasmic domain (residues 55 to 319) (12) (Fig. 1). The periplasmic domain comprises three short regions with an α-helical character that are centered around residues 62 to 67 (H1), 80 to 93 (H2), and 117 to 123 (H3), an unstructured glutamine-rich linker (residues 124 to 242), and a C-terminal globular SPOR domain (residues 243 to 319) that has an affinity for peptidoglycan (55, 60) (Fig. 1).

As with most SR proteins, it is unclear what the essential role of FtsN is. The *ftsN* gene was first identified as a multicopy suppressor of a Ts allele in essential division gene *ftsA* (11). Elevated levels of FtsN were subsequently found to also suppress some Ts alleles in *ftsI*, *ftsK*, and *ftsQ* (11, 18), and even to allow the propagation of cells with a complete lack of FtsK (22, 26) or of FtsEX (48). Depletion of FtsN allows assembly of all the other known essential components into nonconstricting SRs, but the number of ring structures per unit of cell length in FtsN^{-} filaments is two- to threefold lower than in wild-type (WT) cells (9). Bacterial two-hybrid studies suggest that FtsN interacts with several other SR proteins, including FtsA, FtsI (penicillin-binding protein 3 [PBP3]), FtsQ, FtsW, and MtgA

* Corresponding author. Mailing address: Department of Molecular Biology & Microbiology, School of Medicine, Case Western Reserve University, 10900 Euclid Avenue, Cleveland, OH 44106-4960. Phone: (216) 368-1697. Fax: (216) 368-3055. E-mail: pad5@po.cwru.edu.

† Supplemental material for this article may be found at http://jb.asm.org/.

‡ M.A.G., B.L., and F.O.B. contributed equally to this study.

§ Present address: Center for Integrative Genomics, University of Lausanne, Lausanne, Switzerland.

¶ Present address: Department of Microbiology and Molecular Genetics, Harvard Medical School, Boston, MA.

▽ Published ahead of print on 14 August 2009.

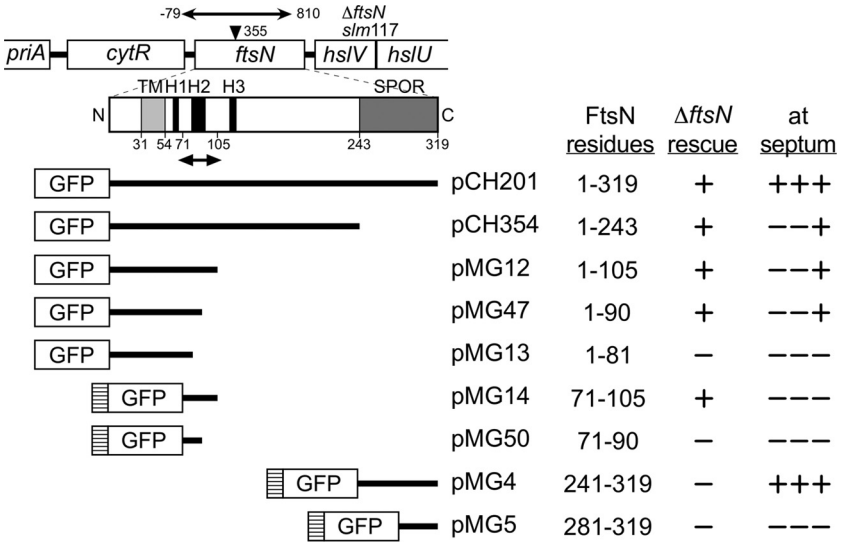

FIG. 1. *E. coli ftsN* locus, FtsN domains, and properties of genetic constructs. Shown are the EZTnKan-2 insertion site in *ftsN*^{slm117} strains and the deletion-replacement in *ftsN*<>*aph* (Δ*ftsN*) strains. Numbers refer to the site of insertion (black triangle) or to the base pairs that were replaced with an *aph* cassette (doubleheaded arrow), counting from the start of *ftsN*. The domain structure of FtsN is illustrated below the *ftsN* gene. Indicated are the transmembrane domain (TM; light gray), helices H1, H2, and H3 (black) in the periplasmic juxtamembrane region, and the C-terminal SPOR domain (^{S}FtsN; dark gray). The small periplasmic peptide that is sufficient for FtsN′s essential function in cell division (^{E}FtsN [see text]) is indicated with the doubleheaded arrow below the domain structure diagram. Also shown are inserts present on plasmids that produce fusions of various portions of FtsN to GFP or ^{TT}GFP under the control of the P_{lac} regulatory region. ^{TT}GFP-fusions contain the TorA signal peptide (hatched box) that is cleaved upon export to the periplasm via the twin arginine transport (Tat) system. Columns indicate the FtsN residues present in each fusion, whether the fusion could (+) or could not (−) compensate for the absence of native FtsN, and whether it accumulated at constriction sites sharply (+++) or poorly (−−+) or appeared evenly distibuted along the periphery of the cell (−−−).

(10, 16, 17, 38). Moreover, it was recently shown that the requirement for FtsN itself can be bypassed in cells producing certain mutant forms of FtsA, which are thought to stabilize the SR to a greater degree than native FtsA (5). These observations are all compatible with a general role of FtsN in stabilizing the ring structure. In addition, it was recently found that FtsN interacts directly with PBP1B, one of the major bifunctional murein synthases in *E. coli*, and that it can stimulate both its transglycosylase and transpeptidase activities in vitro (46). Thus, in addition to stabilizing the SR, FtsN may have a more specific role in modulating septal murein synthesis. Lastly, based on the fact that FtsN is the last known essential protein to join the SR, it is attractive to speculate the protein plays a role in triggering the constriction phase (10, 25). To what degree any of these proposed functions contribute to the essentiality of FtsN remains unclear.

What does seem clear is that the essential activity of FtsN takes place in the periplasm and that residues 139 to 319 are dispensable for its essential function (12, 55). In addition, as residues 1 to 45 are also dispensable for targeting of FtsN to division sites, some portion of the periplasmic domain must also be sufficient to direct the protein to the division apparatus (1).

In a genetic screen for synthetic lethality with *min* (*slm*) (6, 7), we isolated a mutant strain carrying a transposon insertion in codon 119 of *ftsN*. The viability of cells containing this severely truncated *ftsN*^{slm117} allele prompted us to better define the functional domains of FtsN, and we did so by studying the properties of fusions between various portions of FtsN to green fluorescent protein (GFP). To sublocalize a subset of these, we took advantage of the ability of the twin arginine transport system (Tat) to export functional and fluorescent GFP fusions into the periplasm, such that their periplasmic localization could be determined in live cells by fluorescence microscopy (6, 8, 50, 54).

We show that the essential function of FtsN can be performed by a surprisingly small periplasmic peptide of at most 35 residues that is centered around helix H2 but that this essential domain (^{E}FtsN) itself is unlikely to contribute much, if anything, to the accumulation of FtsN at constriction sites. On the other hand, the nonessential periplasmic SPOR domain (^{S}FtsN) localized sharply to these sites by itself, while SPOR-less FtsN derivatives localized poorly, at best. Notably, septal localization of ^{S}FtsN depended on coproduction of ^{E}FtsN, in *cis* or in *trans*, unless cells were provided with the FtsA^{E124A} protein (5) to allow constriction to ensue in the complete absence of ^{E}FtsN. Localization of ^{S}FtsN also depended on the activity of FtsI (PBP3) and the presence of at least one of the periplasmic murein amidases, AmiA, -B, or -C. The results suggest that FtsN joins the division apparatus in a self-enhancing fashion at the time of constriction initiation, which is compatible with a role of the protein in triggering the constriction phase of the division process. In addition, the results, taken together with earlier biochemical work (44, 46, 55), suggest that ^{S}FtsN is recruited to some form of septal murein that accumulates only transiently at sites of active constriction.

In addition to FtsN, *E. coli* produces three proteins of unknown function that also bear a C-terminal SPOR domain (PF05036; Pfam 23) (20). Two of these, DamX and DedD, are inner membrane proteins with the same topology as FtsN, while the third, RlpA, is an outer membrane lipoprotein (43,

TABLE 1. *E. coli* plasmids and phages used in this study

Construct	Relevant genotype[a]	Origin	Source or reference
pAH83	*bla repA*(Ts) *c*I857 λP_R::*xis int* (HK022)	pSC101	29
pBL5	*att*HK022 *bla lacI*^{q} P_{lac}::^{ss}*torA-gfp*	R6K	This work
pBL6	*att*HK022 *bla lacI*^{q} P_{lac}::^{ss}*torA-gfp-ftsN*(241–319)	R6K	This work
pBL12	*cat repA*(Ts) *ftsA*(E124A)	pSC101	This work
pBL28	*bla lacI*^{q} P_{lac}::^{ss}*torA-gfp-damX*$^{338–428}$	ColE1	This work
pBL29	*bla lacI*^{q} P_{lac}::^{ss}*torA-gfp-rlpA*$^{281–362}$	ColE1	This work
pBL34	*bla lacI*^{q} P_{lac}::^{ss}*torA-gfp-cwlC*$^{181–255}$	ColE1	This work
pBL46	*aph repA*(Ts) *araC* P_{BAD}::γ β exo	pSC101	This work
pBL47	*bla lacI*^{q} P_{lac}::*damX*	ColE1	This work
pBL48	*att*HK022 *cat lacI*^{q} P_{lac}::*zipA-gfp*	R6K	This work
pBL49	*att*HK022 *cat lacI*^{q} P_{lac}::^{ss}*torA-gfp*	R6K	This work
pBL50	*att*HK022 *cat lacI*^{q} P_{lac}::^{ss}*torA-gfp-ftsN*(241–319)	R6K	This work
pBL57	*att*HK022 *cat lacI*^{q} P_{lac}::^{ss}*torA-gfp-cwlC*(181–255)	R6K	This work
pCH178	*bla lacI*^{q} P_{lac}::*zipA*$^{1–183}$*-gfp*	ColE1	36
pCH201	*bla lacI*^{q} P_{lac}::*gfp-ftsN*$^{1–319}$	ColE1	31
pCH354	*bla lacI*^{q} P_{lac}::*gfp-ftsN*$^{1–243}$*-le*	ColE1	This work
pCX16	*aadA sdiA*	pSC101	58
pDB280	*cat repA*(Ts) *ftsA*	pSC101	30
pFB184	*bla lacI*^{q} P_{lac}::*sdiA*::*lacZ*	F	4
pFB236	*bla lacI*^{q} P_{lac}::*gfp-dedD*	ColE1	This work
pFB239	*bla lacI*^{q} P_{lac}::*dedD*	ColE1	This work
pFB241	*bla lacI*^{q} P_{lac}::*rlpA-rfp*	ColE1	This work
pFB269	*bla lacI*^{q} P_{lac}::*yfp-damX*	ColE1	This work
pMG4	*bla lacI*^{q} P_{lac}::^{ss}*torA-gfp-ftsN*$^{241–319}$	ColE1	This work
pMG5	*bla lacI*^{q} P_{lac}::^{ss}*torA-gfp-ftsN*$^{281–319}$	ColE1	This work
pMG12	*bla lacI*^{q} P_{lac}::*gfp-ftsN*$^{1–105}$*-le*	ColE1	This work
pMG13	*bla lacI*^{q} P_{lac}::*gfp-ftsN*$^{1–81}$*-le*	ColE1	This work
pMG14	*bla lacI*^{q} P_{lac}::^{ss}*torA-gfp-ftsN*$^{71–105}$*-le*	ColE1	This work
pMG20	*cat araC* P_{BAD}::^{ss}*torA-bfp-ftsN*$^{71–105}$*-le*	pACYC	This work
pMG44	*bla lacI*^{q} P_{lac}::^{ss}*torA-gfp-dedD*$^{140–220}$	ColE1	This work
pMG47	*bla lacI*^{q} P_{lac}::*gfp-ftsN*$^{1–90}$	ColE1	This work
pMG50	*bla lacI*^{q} P_{lac}::^{ss}*torA-gfp-ftsN*$^{71-90}$	ColE1	This work
pMG59	*att*HK022 *bla lacI*^{q} P_{lac}::*gfp-ftsN*$^{1–319}$	R6K	This work
pMG60	*att*HK022 *bla lacI*^{q} P_{lac}::*gfp-ftsN*$^{1–243}$*-le*	R6K	This work
pMLB1113	*bla lacI*^{q} P_{lac}::*lacZ*	ColE1	14
pTB6	*bla lacI*^{q} P_{lac}::^{ss}*torA-gfp*	ColE1	6
pTB8	*bla lacI*^{q} P_{lac}::*minCDE*::*lacZ*	F	6
pTB102	*cat repA*(Ts) *c*I857 λP_R::*int* (HK022)	pSC101	7
pTB222	*att*HK022 *bla lacI*^{q} P_{lac}::*zipA-gfp*	R6K	4
λFB236	*imm*^{21} *bla lacI*^{q} P_{lac}::*gfp-dedD*	λ	This work
λFB241	*imm*^{21} *bla lacI*^{q} P_{lac}::*rlpA-rfp*	λ	This work

[a] In-frame sequences encoding the Tat-targeted signal sequence of TorA (^{ss}*torA*), BFP (*bfp*), YFP (*yfp*), GFPmut2 (*gfp*), mCherry (*rfp*), or the dipeptide LE (*le*) are indicated.

47, 53). We found that all three also accumulate at septal rings and that each of their SPOR domains act as autonomous septal targeting determinants. Moreover, phenotypes of the mutants indicate that both DamX and DedD contribute to the cell constriction process, leading to classification of these proteins as new nonessential division proteins.

A SPOR domain is predicted to be present in at least 1,650 (putative) proteins from over 500 bacterial species (PF05036; Pfam 23) (20), raising the question as to how far SPOR properties have been conserved. We find that the SPOR domain of CwlC, a *Bacillus subtilis* murein amidase that is active during late stages of sporulation (39, 44), also accumulates sharply at division sites in *E. coli*.

Our results predict that many other bacterial SPOR domain proteins specifically recognize the same or closely related target molecule(s) that accumulates transiently at sites of cell constriction. This is supported by a very recent study showing that SPOR domain proteins from *Burkholderia thailandensis*, *Caulobacter crescentus*, and *Myxococcus xanthus* accumulate at cell constriction sites as well (45).

MATERIALS AND METHODS

Plasmids and phages. Relevant plasmids and phages are listed in Table 1. Plasmids pMLB1113 (14), pDB280 (30), pKD3, pKD13, and pKD46 (13), pAH68 and pAH83 (29), pDB391 (32), pCH157 (40), pCH201 (31), pCH151 (8), pTB6 and pTB8 (6), pTB102 (7), pMG36 and pMLB1113ΔH (24), pCH181, pCH233 and pCH268 (3), and pCH310, pFB114, pFB184, pTB98, and pTB222 (4) have been described before.

Unless indicated otherwise, MG1655 or TB28 chromosomal DNA was used as the template in amplification reactions. Sites of interest (e.g., relevant restriction sites or those allowing for targeted recombination) are underlined in the primer sequences below.

Plasmid pBL5 (*att*HK022 *bla lacI*^{q} P_{lac}::^{TT}*gfp*) was obtained by replacing the 2,343-bp ApaI-MfeI fragment of pTB222 with the 1,374-bp ApaI-MfeI fragment of pTB6.

For pBL6 (*att*HK022 *bla lacI*^{q} P_{lac}::^{TT}*gfp-ftsN*$^{241–319}$), the 2,513-bp ApaI-HindIII fragment of pTB222 was replaced with the 1,806-bp ApaI-HindIII fragment of pMG4.

For pBL12 [*cat repA*(Ts) *ftsA*^{E124A}], an *ftsA* plasmid that will be described elsewhere (pCH316), was mutagenized by the QuikChange method (Stratagene) with primers 5′-CGGTGCGTGTGCGCGATGCGCATCGTGTGCTGCATGTG-3′ and its reverse complement. This yielded pBL14, in which codon 124 of *ftsA* is changed from GAG to GCG, simultaneously resulting in a diagnostic FspI site (underlined). pBL12 was then obtained by replacing the 852-bp BglII-AscI fragment of pDB280 [*cat repA*(Ts) *ftsA*] with that of pBL14.

To construct pBL28 (P_{lac}::^{TT}*gfp-damX*$^{338–428}$), primers 5′-AGTTGGATCCTTGAAATCGGCACCGTCCAGCC-3′ and 5′-CCCAAGCTTTTACTTCAGATCGGCCTGTACC-3′ were used to amplify a fragment of pFB269 (P_{lac}::*yfp-damX*). The product was digested with BamHI and HindIII, and the 275-bp fragment was used to replace the 802-bp BamHI-HindIII fragment of pCH282 (P_{lac}::^{TT}*gfp-ftsN*$^{55–319}$).

For pBL29 (P_{lac}::^{TT}*gfp-rlpA*$^{281–362}$), pMG40 (P_{lac}::*rlpA*) was used as a template in a PCR with primers 5′-GAACAGATCTCAAGCCGTCTCGCAAAGCGCCAGC-3′ and 5′-CGGAAGCTTTTACTGCGCGGTAGTAATAAATGACTGTAATTGGGC-3′. The product was treated with BglII and HindIII, and the resulting 254-bp fragment was used to replace the 802-bp BamHI-HindIII fragment of pCH282.

For pBL34 (P_{lac}::^{TT}*gfp-cwlC*$^{181–255}$), primers 5′-GCAGGGATCCAGCTCAGGGTTATATAAGG-3′ and 5′-CCAAGCTTATGATTCTAGGATCACAATAGCGTCAAAG-3′ were used to amplify a chromosomal fragment of *Bacillus subtilis* strain PY79 (kindly provided by Peter Setlow). The product was digested with BamHI and HindIII, and the resulting 228-bp fragment was used to replace the 802-bp BamHI-HindIII fragment of pCH282.

To obtain pBL46 [*aph repA*(Ts) *araC* P_{BAD}::γ β *exo*], the *bla* gene on pKD46 (13) was replaced with *aph* by λ-red recombineering (13, 61). The *aph* cassette of pKD13 was amplified with primers 5′-GTGAATGATGTAGCCGTCAAGTTGTCATAATAAATCGATGACGCTGCCGCAAGCACTCAG-3′ and 5′-TTTGGTCATGAGATTATCAAAAAGGATCTTCACCTAGATCGATCCCCTTATTAGAAGAAC-3′, resulting in a 935-bp fragment with end sequences homologous to those flanking *bla* on pKD46. Recombination of this fragment with the plasmid in strain TB10/pKD46 yielded TB10/pBL46.

For pBL47 (P_{lac}::*damX*), the *damX* gene was amplified with primers 5′-GCTCTAGAGCATTAACCTTTTAGTGGGGTG-3′ and 5′-CGCTCGAGTTACTTCAGATCGGCCTGTAC-3′. The product was treated with XbaI and XhoI, and the resulting 1,318-bp fragment was used to replace the 1,099-bp XbaI-XhoI fragment of pCH310.

To obtain pBL48 (*att*HK022 *cat lacI*^{q} P_{lac}::*zipA-gfp*), the *bla* gene on the integrated form of pTB98 (iTB98) was replaced with *cat* by recombineering. The *cat* cassette of pKD3 was amplified with primers 5′-ATGAGACAATAACCCTGATAAATGCTTCAATAATATTGAAATGAATATCCTCCTTAGTTCC-3′ and 5′-TTAAAAATGAAGTTTTAAATCAATCTAAAGTATATATGAGGTGTAGGCTGGAGCTGCTTCG-3′, resulting in a 1,091-bp fragment with end sequences homologous to those flanking *bla* on pTB98. Recombination of this fragment with the integrated plasmid in strain TB28(iTB98)/pBL46 and subsequent curing of pBL46 by growth at 37°C yielded TB28(iBL48). The excised and replicative form of the plasmid was next obtained by preparation of a P1 lysate and infection of strain BW23473/pAH83, essentially as described previously (29).

Plasmids pBL49 (*att*HK022 *cat lacI*^{q} P_{lac}::^{TT}*gfp*) and pBL50 (*att*HK022 *cat lacI*^{q} P_{lac}::^{TT}*gfp-ftsN*$^{241–319}$) were obtained as described for pBL48 above, except that the *cat* fragment was recombined with strains TB28(iBL5)/pBL46 and TB28(iBL6)/pBL46, respectively.

For pBL57 (*att*HK022 *cat lacI*^{q} P_{lac}::^{TT}*gfp-cwlC*$^{181–255}$), the 228-bp BamHI-HindIII fragment of pBL34 was used to replace the 243-bp BamHI-HindIII fragment of pBL50.

To create pCH276 (P_{lac}::*gfp-ftsN*$^{1–123}$), primers 5′-CGCAGCTAGCAAAGGAGAAGAACTTTTCACTGG-3′ and 5′-CGAACTCGAGAAGCTGACGTTGTTCTGGTGTCAG-3′ were used to amplify a 1,139-bp fragment of pCH201 (P_{lac}::*gfp-ftsN*). This fragment was digested with NheI (internal to fragment) and XhoI (underlined), and the 411-bp product was used to replace the 1,119-bp NheI-XhoI fragment of pCH181 (P_{lac}::*gfp-minD minE-le*).

Plasmid pCH282 (P_{lac}::^{TT}*gfp-ftsN*$^{55–319}$) was created in several steps. Primers 5′-CTGTACGGATCCACGCATCACAAGAAAGAAGAGTCC-3′ and 5′-TGAGAAGCTTAACCCCCGGCGGCGAG-3′ were used to amplify a 989-bp fragment of pCH201, which was digested with BamHI and HindIII. The 802-bp product was used to replace the 25-bp BamHI-HindIII fragment of pET21A, yielding pCH231 (P_{T7}::*ftsN*$^{55–319}$). The 835-bp NheI-HindIII fragment of pCH231 was subsequently used to replace the 66-bp NheI-HindIII fragment of pTB6 (P_{lac}::^{TT}*gfp*), yielding pCH282.

For pCH288 (P_{lac}::^{TT}*gfp-ftsN*$^{55–123}$), primers 5′-CTGTACGGATCCACGCATCACAAGAAAGAAGAGTCC-3′ and 5′-GACGTTGTAAAACGACGGCCAGTG-3′ were used to amplify a 268-bp fragment of pCH276, and this fragment was treated with BamHI and HindIII (internal to fragment). The 230-bp product was used to replace the 802-bp BamHI-HindIII fragment of pCH282, yielding pCH288.

Plasmid pCH305 (P_{lac}::*yfp-mreD-le*) encodes an *E. coli* codon-optimized yellow fluorescent protein (YFP) and was used as a cloning vehicle. To create it, *yfp* was amplified from pNR14 (kindly supplied by Nick Renzette and Steven Sandler) using primers 5′-TTAACCATGGCCGACTCTGGTGACTACCTTTGGTTATGGTCTG-3′ and 5′-TCATGCTAGCTTTGTAGAGCTCATCCATGCCGTGCGTGATACC-3′. The 563-bp product was treated with NcoI and NheI, and the 549-bp fragment was used to replace the 549-bp NcoI-NheI fragment of pCH303 (P_{lac}::*gfp-mreD-le*). The latter was obtained by removal of the SacI site in pCH233 (3) by digestion with the enzyme, treatment with T4 DNA polymerase, and ligation of the blunted ends.

For pCH354 (P_{lac}::*gfp-ftsN*$^{1–243}$), we used primers 5′-ATGACTGGTGGACAGCAAATGG-3′ and 5′-GGCGCTCGAGTTTTTTCTCCGCCGTCGGTTTTGG-3′ to amplify a 781-bp fragment of pCH201. The fragment was treated with BamHI (internal to fragment) and XhoI (underlined), and the 744-bp product was used to replace the 330-bp BamHI-XhoI fragment of pMG12.

For pFB236 (P_{lac}::*gfp-dedD*), *dedD* was amplified with primers 5′-CGCGGATCCGTGGCAAGTAAGTTTCAGAATCGGTTAGTGGGC-3′ and 5′-CCCAAGCTTTTAATTCGGCGTATAGCCCATTACCACGCC-3′. The product was treated with BamHI and HindIII, and the resulting 669-bp fragment was used to replace the 1,039-bp BamHI-HindIII fragment of pFB114 (P_{lac}::*gfp-mreB*$^{5–347}$).

For pFB239 (P_{lac}::*dedD*), *dedD* was amplified with primers 5′-GCTCTAGAGCACATGTCATGGAAGTGATTGACGCG-3′ and 5′-CCCAAGCTTTTAATTCGGCGTATAGCCCATTACCACGCC-3′. The product was treated with XbaI and HindIII, and the resulting 706-bp fragment was used to replace the 1,974-bp XbaI-HindIII fragment of pFB211 (P_{lac}::*mreC-rfp*), a pMLB1113 derivative that will be detailed elsewhere.

For pFB241 (P_{lac}::*rlpA-rfp*), *rlpA* was amplified with primers 5′-GCTCTAGAGAAAATGTTGTCGAAAAGCGTGTAAGAGGTGCGC-3′ and 5′-CCGCTCGAGCTGCGCGGTAGTAATAAATGACTGTAATTGGGC-3′. The product was treated with XbaI and XhoI, and the resulting 1,127-bp fragment was used to replace the 584-bp XbaI-XhoI fragment of pMG36 (P_{lac}::*pal-rfp*).

For pFB269 (P_{lac}::*yfp-damX*), *damX* was amplified with primers 5′-GCGGATCCGAATGGATGAATTCAAACCAGAAGACGAGC-3′ and 5′-CCCAAGCTTTTACTTCAGATCGGCCTGTACC-3′. The product was treated with BamHI and HindIII, and the resulting 1,294-bp fragment was ligated to the 8,406-bp BamHI-HindIII fragment of pCH305 (P_{lac}::*yfp-mreD-le*).

For pMG4 (P_{lac}::^{TT}*gfp-ftsN*$^{241–319}$), primers 5′-AGAGGGATCCGAGAAAAAGACGAACGCCGCTGG-3′ and 5′-TGAGAAGCTTAACCCCCGGCGGCGAG-3′ were used to amplify a 258-bp fragment of pCH201. The product was digested with BamHI and HindIII, and the 244-bp fragment was used to replace the 802-bp BamHI-HindIII fragment of pCH282.

For pMG5 (P_{lac}::^{TT}*gfp-ftsN*$^{281–319}$), primers 5′-GTAAGGATCCAATGGCTGGAATCGTGTGGTC-3′ and 5′-TGAGAAGCTTAACCCCCGGCGGCGAG-3′ were used to amplify a 138-bp fragment of pCH201. The product was digested with BamHI and HindIII, and the 124-bp fragment was used to replace the 802-bp BamHI-HindIII fragment of pCH282.

Plasmids pMG12 (P_{lac}::*gfp-ftsN*$^{1–105}$), pMG13 (P_{lac}::*gfp-ftsN*$^{1–81}$), and pMG47 (P_{lac}::*gfp-ftsN*$^{1–90}$) were constructed in a similar fashion as pCH276 (see above), using primers 5′-CGCAGCTAGCAAAGGAGAAGAACTTTTCACTGG-3′ (in each case) and 5′-GCCACTCGAGACCGGCAGAAGGTTCTGTGGGCGC-3′ (pMG12), 5′-AGCGCTCGAGTTCTTCTGGTTTTGGTGGTAGTCCGTTTCC-3′ (pMG13), or 5′-ATTTCTCGAGCTCTTTAATGTAGCGCCAGCGTTCTTCTGG-3′ (pMG47).

For pMG14 (P_{lac}::^{TT}*gfp-ftsN*$^{71–105}$), primers 5′-GCCAGGATCCACCGGAAACGGACTACCACCAAAACC-3′ and 5′-GACGTTGTAAAACGACGGCCAGTG-3′ were used to amplify a 170-bp fragment of pMG12. The product was digested with BamHI and HindIII (internal to fragment), and the 140-bp fragment was used to replace the 802-bp BamHI-HindIII fragment of pCH282.

Plasmid pMG15 (P_{lac}::^{TT}*bfp-ftsN*$^{71–105}$) was obtained by replacing the 549-bp NcoI-NheI fragment of pMG14 with that of pDB391 (P_{lac}::*bfp-minD*).

For pMG20 (P_{BAD}::^{TT}*bfp-ftsN*$^{71–105}$), primers 5′-ATTTTCTAGAATTAAGAAGGAGATATACCATGAACAATAACGATCTCT-3′ and 5′-AAAGGGGGATGTGCTGCAAG-3′ were used to amplify a 1,140-bp fragment from pMG15. The product was digested with XbaI and SalI (internal to fragment), and the 1,025-bp fragment was used to replace the 2,216-bp XbaI-SalI fragment of pCH264 (P_{BAD}::*gfp-ftsA*), a derivative of pBAD33 (28) that will be detailed elsewhere.

For pMG44 (P_{lac}::^{TT}*gfp-dedD*$^{140–220}$), pFB239 was used as a template in a PCR with primers 5′-CGGGATCCACGGGTAAAGCCTATGTTGTGC-3′ and 5′-CCCAAGCTTTTAATTCGGCGTATAGCCCATTACCACGCC-3′. The

TABLE 2. *E. coli* strains used in this study

Strain[a]	Relevant genotype[b]	Source or reference
BL7	TB28, *amiB<>aph*	This work
BL8	TB28, *amiB<>frt*	This work
BL9	TB28, *amiC<>aph*	This work
BL10	TB28, *amiB<>frt amiC<>aph*	This work
BL11	TB28, *amiC<>aph amiA<>cat*	This work
BL12	TB28, *amiA<>cat amiB<>frt amiC<>aph*	This work
BL18	TB28, $ftsA^{E124A}$	This work
BL20*	TB28, $ftsA^{E124A}$ *ftsN<>aph*	This work
BL25	TB28, *amiA<>cat*	This work
BL38	TB28, *damX<>cat*	This work
BL40	TB28, *dedD<>frt damX<>cat*	This work
BL41	TB28, *rlpA<>frt dedD<>cat*	This work
BL43	TB28, *damX<>cat* $ftsN^{slm117}$	This work
BL44	TB28, *rlpA<>frt* $ftsN^{slm117}$	This work
BL45	TB28, *rlpA<>frt damX<>cat* $ftsN^{slm117}$	This work
BL48	TB28, *rlpA<>frt damX<>frt dedD<>cat*	This work
BW23473	Δ(*lacIZYA-argF*)*U169 rph-1 rpoS396*^{Am} *robA1 creC510 hsdR514* Δ*endA9 uidA*(Δ*MluI*)::pir^{WT} *recD1014 recA1*	29
CH31*	TB28, P_{ftsN}<>(*aph araC* P_{BAD}) (*aph araC* P_{BAD}::*ftsN*)	This work
CH34*	TB28, *ftsN<>aph*	This work
DY329	*rph*1 IN(*rrnD-rrnE*) Δ(*argF-lac*)*U169 nadA*::Tn*10 gal490* λ*c*I857 Δ(*cro-bioA*)	61
FB55	TB28, *dedD*::EZTnKan-2	This work
FB70	TB28, *rlpA<>cat*	This work
FB71	TB28, *dedD<>cat*	This work
MG13	TB28 *rlpA<>frt*	This work
MG14	TB28 *dedD<>frt*	This work
MG19*	TB28 *dedD<>frt* $ftsN^{slm117}$[c]	This work
MG1655	*ilvG rfb50 rph1*	27
Slm117	TB43, $ftsN^{slm117}$ (*ftsN*::EZTnKan-2)	This work
TB10	MG1655, *nadA*::Tn*10* λ*c*I857 Δ(*cro-bioA*)	36
TB28	MG1655, *lacIZYA<>frt*	8
TB43	TB28, *minCDE<>frt*	7
TB54*	DY329, P_{ftsN}<>(*aph araC* P_{BAD}) (*aph araC* P_{BAD}::*ftsN*)	8
TB77[c]	TB28, $ftsN^{slm117}$	This work

[a] Note that strains marked with an * required an appropriate plasmid, phage, and/or inducer for survival.
[b] The symbol <> denotes DNA replacement, and *frt* is a scar sequence remaining after eviction of an *aph* or *cat* cassette by FLP recombinase (13, 61).
[c] The slm117 allele (*ftsN*::EZTnKan-2) encodes the first 118 residues of FtsN, followed by the nonsense peptide LSLIHISTLKLACLQVDSRGSPPRLMRALL.

product was treated with BamHI and HindIII, and the resulting 252-bp fragment was used to replace the 802-bp BamHI-HindIII fragment of pCH282.

For pMG50 (P_{lac}::^{TT}*gfp-ftsN*$^{71–90}$), primers 5′-CGCAGCTAGCAAAGGAGAAGAACTTTTCACTGG-3′ and 5′-ATTTCTCGAGCTCTTTAATGTAGCGCCAGCGTTCTTCTGG-3′ were used to amplify an 821-bp fragment of pMG14. The product was digested with NcoI (internal to fragment) and XhoI, and the 642-bp fragment was used to replace the 789-bp NcoI-XhoI fragment of pCH288.

For pMG59 (*att*HK022 *bla lacI*^{q} P_{lac}::*gfp-ftsN*$^{1–319}$), the 1,745-bp XbaI-HindIII fragment of pCH201 was used to replace the 1,778-bp XbaI-HindIII fragment of pTB222 (*att*HK022 *bla lacI*^{q} P_{lac}::*zipA-gfp*).

For pMG60 (*att*HK022 *bla lacI*^{q} P_{lac}::*gfp-ftsN*$^{1–319}$), the 1,539-bp XbaI-HindIII fragment of pCH354 was used to replace the 1,778-bp XbaI-HindIII fragment of pTB222.

λFB236 (P_{lac}::*gfp-dedD*) and λFB241 (P_{lac}::*rlpA-rfp*) were obtained after crossing pFB236 and pFB241, respectively, with λNT5 (*imm*^{21}), as described previously (14).

Strains. Relevant *E. coli* strains are listed in Table 2.

Amidase knockout strains BL7 to BL12 and BL25 were created by λRed-mediated recombineering (13, 61). A 1,093-bp *amiA<>cat* fragment was generated by amplifying the *cat* cassette of pKD3 using primers 5′-CCGTCGTAACGGATTACGCGATACGATATAACATCTGGACCATATGAATATCCTCCTTAG-3′ and 5′-TAACAGCCGTTCTTCTTCCGGGTTGGTGATAAACGAGGTGTGTAGGCTGGAGCTGCTTCG-3′, while the *aph* cassette of pKD13 was amplified using 5′-CTGGCGCGTTTAGCCGGTTAACCTTTGAAAGGTGGCGGGAATTCCGGGGATCCGTCGACC-3′ and 5′-CCATACGGAAGCGCCAGTCGCACTGCGGTTCGGTGCGGCGTGTAGGCTGGAGCTGCTTCG-3′ to yield a 1,383-bp *amiB<>aph* fragment, or by using 5′-GTTTCCGGTCAAATTAGTCGTTTACTTGTTACACAGCTTAATTCCGGGGATCCGTCGACC-3′ and 5′-CTGGTCTCCCATAAAAAAGCGCCATTCAGCGCCTTTTTAGTGTAGGCTGGAGCTGCTTCG-3′ to generate a 1,383-bp *amiC<>aph* fragment (chromosomal sequences underlined). Each fragment was recombined with the chromosome of TB10, resulting in three strains that served as donors for transduction of each knockout allele into TB28, to generate BL7 (*amiB<>aph*), BL9 (*amiC<>aph*), and BL25 (*amiA<>cat*). In BL25, *cat* replaces 751 bp of the *amiA* gene (from bp −25 to +726), while *aph* replaces 811 bp of the *amiB* gene (from bp +2 to +813) in BL7 and the entire *amiC* gene (from bp −22 to +1343) in BL9. FLP-mediated eviction of *aph* (13) from BL7 yielded BL8 (*amiB<>frt*), and transduction of *amiC<>aph* into BL8 resulted in BL10. Transduction of *amiA<>cat* into BL9 and BL10 then gave rise to BL11 and BL12, respectively.

Strain BL18 ($ftsA^{E124A}$) was obtained by exchance of the chromosomal wild-type *ftsA* allele of strain TB28 with the $ftsA^{E124A}$ allele on plasmid pBL12 [*cat repA*(Ts) $ftsA^{E124A}$] (Table 1), using the method of Hamilton et al. (33). BL18 was transformed with pBL12, and transduction of the *ftsN<>aph* allele from CH34/pCH201 yielded BL20/pBL12. Strains BL20(iBL5)/pBL12 and BL20(iBL6)/pBL12 were obtained by transduction of the integrated forms of pBL5 and pBL6 from TB28(iBL5) and TB28(iBL6), respectively, into BL18/pBL12 prior to the introduction of *ftsN<>aph*.

For BL38 (*damX<>cat*), the *cat* cassette of pKD3 was amplified using primers 5′-TGCAACGTGGTAAGCATTAACCTTTTAGTGGGGTGTTAACCATATGAATATCCTCCTTAG-3′ and 5′-CGTAGAAGTCGCAGCCGGTGCCTTCGTGCTCGCCACAGGGTGTAGGCTGGAGCTGCTTCG-3′. Recombination of the 1,093-bp fragment with the chromosome of TB10/pFB269 yielded BL36/pFB269, in which bp 1 to 869 of *damX* were replaced with a *cat* gene that was transcribed in the same direction, leaving promoters P4 and P5 of the downstream *dam* gene intact (42). Transduction of *damX<>cat* from the latter to TB28 then yielded BL38.

BL40 was obtained by transduction of *damX<>cat* from BL36/pFB269 to

MG14, BL41 was obtained by transduction of *dedD*<>*cat* from FB71/pFB239 to MG13, BL42 (*rlpA*<>*frt damX*<>*cat*) was obtained by transduction of *damX*<>*cat* from BL36/pFB269 to MG13, BL43 was obtained by transduction of *ftsN*::EZTnKan-2 (*ftsN*^{slm117}) from TB77 to BL38, BL44 was obtained by transduction of *ftsN*^{slm117} from TB77 to MG13, BL45 was obtained by transduction of *ftsN*^{slm117} from TB77 to BL42, BL47 (*rlpA*<>*frt damX*<>*frt*) was obtained by eviction of *cat* from BL42, and BL48 was obtained by transduction of *dedD*<>*cat* from FB71/pFB239 to BL47.

Strain CH31(*aph araC* P_{BAD}::*ftsN*) was obtained by transduction of P_{ftsN}<>(*aph araC* P_{BAD}) from TB54 to TB28 and required arabinose for survival.

To create CH34 (Δ*ftsN*), the *aph* cassette of pKD13 was amplified with primers 5′-TCCGGGGATCAACACGCGCGTTACCTTAAAGTAAACCTTTGTGTAGGCTGGAGCTGCTTC3′ and 5′-TCCAGCCATTGTTGGTGGTGATTTTCGAGTCAAAGCCTTCATTCCGGGGATCCGTCGACC-3′, resulting in a 1,384-bp fragment with end sequences homologous to the chromosomal *ftsN* locus (underlined). Recombination of this fragment with the chromosome of TB10/pCH201 yielded CH33/pCH201, in which 890 bp of the *ftsN* locus (from bp −80 to bp +810) was replaced with *aph*, whose transcription was directed away from the downstream *hslV* gene. Transduction of *ftsN*<>*aph* from CH33/pCH201 to TB28/pCH201 yielded CH34/pCH201.

Strain FB55 (*dedD*::EZTnKan-2) resulted from a new screen we recently described for cell shape/division mutants in which an increased level of FtsZ provides a selective advantage (4). Strain Rod2361/pFB184 (Δ*lacIZYA dedD*::EZTnKan-2/*bla lacI*^{q} P_{lac}::*sdiA*::*lacZ*) was recovered as a solid blue colony after plating an EZTnKan-2 transposon library of host strain TB28/pFB184 (Δ*lacIZYA dedD*::EZTnKan-2/*bla lacI*^{q} P_{lac}::*sdiA*::*lacZ*) at room temperature on LB agar supplemented with isopropyl-β-D-thiogalactopyranoside (IPTG) and 5-bromo-4-chloro-3-indolyl-β-D-galactopyranoside (X-Gal) (LB-IX), as described previously (4). Mapping the EZTnKan-2 insertion site as before (6) revealed that the transposon had inserted just after bp 48 of *dedD*. Subsequent tests showed that extra FtsZ is not essential for viability of the mutant but provides a modest advantage by reducing the average length of cell chains formed by *dedD* mutants (data not shown). FB55 was obtained by transduction of *dedD*::EZTnKan-2 to TB28.

For FB70 (*rlpA*<>*cat*), the *cat* cassette of pKD3 was amplified with primers 5′-ATGCGTAAGCAGTGGCTCGGGATCTGCATCGCGGCAGGAATGCTCGCGGCTGTGTAGGCTGGAGCTGCTTCG-3′ and 5′- CTGCGCGGTAGTAATAAATGACTGTAATTGGGCTTCGGTTTGCAAACGTTTTAGTTCCTATTCCGAAGTTCC-3′, yielding a 1,099-bp fragment with end sequences homologous to the chromosomal *rlpA* locus (underlined). Recombination with the chromosome of TB10/pCX16 yielded FB69/pCX16, in which 986 bp of the *rlpA* gene (from bp +51 to bp +1036) was replaced with *cat* and transcription of the latter was directed away from the downstream *dacA* gene. Transduction of *rlpA*<>*cat* from FB69/pCX16 to TB28 resulted in FB70.

For FB71 (*dedD*<>*cat*), the *cat* cassette of pKD3 was amplified with primers 5′-CGCACATGTCATGGAAGTGATTGACGCGAGGAGAAGCGGTGGCAAGTAAGTAATGTGTAGGCTGGAGCTGCTTCG-3′ and 5′-TTAATTCGGCGTATAGCCCATTACCACGCCACTTAAGCCAGAAAGTTGCTTTAGTTCCTATTCCGAAGTTCC-3′, resulting in a 1,102-bp fragment with end sequences homologous to the chromosomal *dedD* locus (underlined). Recombination of this fragment with the chromosome of TB10/pCX16 yielded FB68/pCX16, in which 598 bp of the *dedD* gene (from bp +14 to bp +612) was replaced with *cat* and transcription of the latter was directed away from the downstream *cvpA* gene. Transduction of *dedD*<>*cat* from FB68/pCX16/pFB239 to TB28 resulted in FB71.

Strains MG13 and MG14 were obtained by eviction of *cat* from FB70 and FB71, respectively.

Strain MG19(λFB236) was obtained by transduction of *ftsN*::EZTnKan-2 (*ftsN*^{slm117}) from TB77 into MG14(λFB236) with selection on LB plates containing 20 μg/ml kanamycin and 100 μM IPTG.

Strain Slm117/pTB8 (Δ*lacIZYA* Δ*minCDE ftsN*::EZTnKan-2/*bla lacI*^{q} P_{lac}::*minCDE lacZ*) was recovered as a solid blue colony after plating an EZTnKan-2 transposon library of host strain TB43/pTB8 (Δ*lacIZYA* Δ*minCDE*/*bla lacI*^{q} P_{lac}::*minCDE lacZ*) at 30°C on LB-IX, as described previously (7). Restreaking of the colony on LB-IX gave rise to both solid blue (Min$^+$) as well as solid white (Min$^-$) colonies, and the latter were still about half the size of the former. This indicated that, relative to previously described *slm* alleles (6, 7), the *ftsN*^{slm117} lesion conferred a more subtle growth defect on Min$^-$ cells. The exact site of the EZTnKan-2 insertion was determined as described before (6).

Strain TB77 (*ftsN*^{slm117}) was obtained by transduction of *ftsN*::EZTnKan-2 from Slm117 to TB28.

Growth conditions. Unless stated otherwise, cells were grown at 30°C in LB (0.5% NaCl) medium or in M9 minimal medium supplemented with 0.2% Casamino Acids, 50 μg/ml L-tryptophan, 50 μM thiamine, and 0.2% of either glucose (M9-glucose) or maltose (M9-maltose). When appropriate, medium was supplemented with 50 μg/ml ampicillin (Amp), 50 μg/ml spectinomycin (Spec), 20 μg/ml kanamycin (Kan), 25 μg/ml chloramphenicol (Cam), or 12.5 μg/ml tetracycline (Tet). Amp and Cam concentrations were reduced to 15 and 10 μg/ml, respectively, when cells carried *bla* or *cat* integrated in the chromosome. Other details are specified below in the text.

Microscopy. MG13(λFB241) [Δ*rlpA*(P_{lac}::*rlpA-rfp*)] cells (see Fig. 10B and C, below) were imaged on a Nikon 90i microscope equipped with a 100× (1.45 numerical aperture) oil objective, an X-Cite 120 fluorescence illuminator (EXFO), a red fluorescent protein (RFP)-specific filter set (532- to 587-nm excitation, 595-nm dichroic mirror, 608- to 683-nm barrier), and a Photometrics QuantEM:512SC back-illuminated electron-multiplying charge-coupled-device camera. All other imaging was performed on a Zeiss Axioplan-2 microscope system as previously described (35). Live cells were imaged on pads of 1.0 or 1.2% agarose with 0.5% NaCl.

Other methods. Cell dimension measurements and Western analyses with anti-GFP antibodies (Rockland) were done essentially as described before (3, 8).

RESULTS

Isolation and characterization of a transposon insertion allele (*ftsN*^{slm117}) of the essential division gene *ftsN*. In synthetic lethality screens for transposon insertions that are particularly detrimental in the absence of a functional Min system (6, 7), we recovered a mutant strain (Slm117) (Table 2) in which EZTnKan-2 disrupts *ftsN* at codon 119. Consequently, the FtsN^{slm117} peptide still contains the cytoplasmic (FtsN$^{1–30}$), transmembrane (FtsN$^{31–54}$), and periplasmic H1 (~FtsN$^{62–67}$) and H2 (~FtsN$^{80–93}$) portions of native FtsN, but it lacks most of H3 (~FtsN$^{117–123}$) and all of the linker (FtsN$^{124–242}$) and C-terminal SPOR (FtsN$^{243–319}$) domains (Fig. 1). Since *ftsN*^{slm117} cells are viable, this further narrowed the minimal essential domain of FtsN (^{E}FtsN) as previously inferred from complementation experiments (55). Although capable of growing at normal rates, cells carrying the *ftsN*^{slm117} allele did show a distinct division phenotype. When TB77 (*ftsN*^{slm117}) cells were grown in LB medium, many formed chains of two or more cell units (Fig. 2A and Table 3), and this division defect became more pronounced when cells were grown in M9 minimal medium (Fig. 2B). The absence of a functional Min system was not lethal to *ftsN*^{slm117} cells but, consistent with recovery of the insertion in the *slm* screen, further aggravated their chaining/filamentation phenotype (data not shown).

Two possible causes of cell chaining are inefficient splitting of septal murein (e.g., in *ami* or *envC* mutants) or inefficient tethering of the outer membrane (OM) to the freshly separated septal murein layers (e.g., in *tol-pal* mutants) (24, 34, 49). Both types of defect result in a delayed invagination of the OM and, therefore, in a localized increase in the intermembrane distance at sites of constriction. At least in the case of *envC* and *tol-pal* chains, this can be readily detected by ring-like accumulations of periplasmic Tat-targeted GFP (^{TT}GFP) at these sites (6, 24). In contrast, we detected no obvious ^{TT}GFP "rings" in chains of TB77/pTB6 cells (Fig. 2E), indicating that *ftsN*^{slm117} cells do not suffer a gross delay in OM invagination. In turn, this suggests that the three envelope layers still invaginate coordinately in *ftsN*^{slm117} cells but that the entire process takes significantly longer to complete than normal.

The essential function(s) of FtsN is carried out by a small periplasmic peptide centered about helix H2. Previous work showed that FtsN variants that either lacked the first 55 (12) or

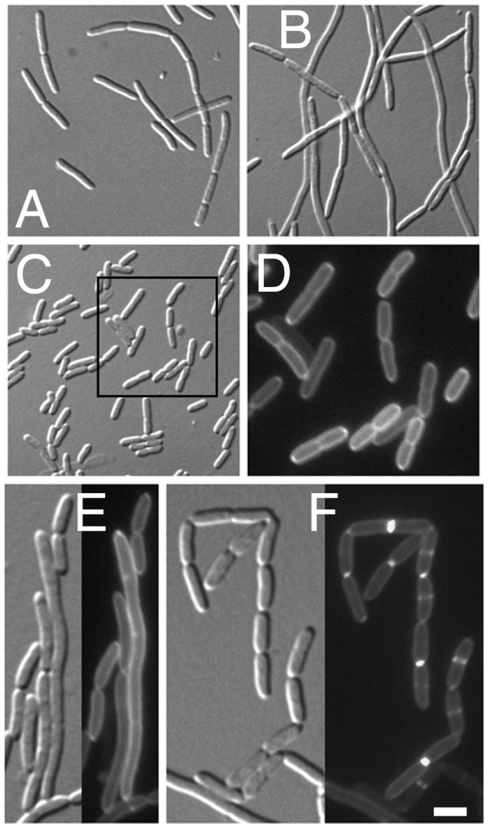

FIG. 2. Division phenotypes of *ftsN*^{slm117} cells. Shown are cells of strain TB77 (*ftsN*^{slm117}) harboring pMLB1113 (vector) (A and B), pMG14 (P_{lac}::^{TT}*gfp-ftsN*$^{71–105}$) (C and D), pTB6 (P_{lac}::^{TT}*gfp*) (E), or pMG4 (P_{lac}::^{TT}*gfp-ftsN*$^{241–319}$) (F). Cells were grown at 30°C to an optical density at 600 nm of 0.6 to 0.8 in LB (A) or in M9-glucose minimal medium (B to F) supplemented with 5 μM (E and F) or 50 μM (A to D) IPTG and imaged live. The square in panel C corresponds to the fluorescence image in panel D. Panels E and F each show corresponding DIC (left) and fluorescence (right) images. Note the even distribution of fluorescence along the cell periphery in panels D and E, in contrast to the sharp accumulation of ^{TT}GFP-^{S}FtsN at constriction sites in panel F. Bar, 2 μm (D to F) or 4 μm (A to C).

the last 181 (55) residues were still capable of carrying out its essential function in cell division. Together with the viability of *ftsN*^{slm117} cells, this indicated that the essential part of FtsN (^{E}FtsN) might be confined to a small periplasmic juxtamembrane peptide of less than 65 residues.

To test this prediction, we performed complementation analyses with plasmids producing fusions of GFP to various portions of FtsN. The plasmids were derivatives of pMLB1113, and the synthesis of fusions was placed under the control of the *lac* regulatory region of the vector (Fig. 1; Table 1). In one assay for FtsN function, plasmids were tested for their ability to correct the division defect of the FtsN depletion strain CH31 (*araC* P_{ara}::*ftsN*). The native *ftsN* promoter region in this strain is replaced with that of *araBAD*, such that *ftsN* transcription from the chromosome depends on the presence of arabinose in the medium (8). In a more stringent assay, plasmids were introduced in the wild-type strain TB28, and transformants were tested for their ability to survive P1-mediated introduction of a chromosomal *ftsN*<>*aph* (Δ*ftsN*) knockout allele in the presence of IPTG. For each fusion capable of rescuing Δ*ftsN* cells, the minimal concentration of IPTG yielding cells of close to normal size was then determined.

As summarized in Fig. 1, production of GFP-FtsN$^{1–319}$ (full length), GFP-FtsN$^{1–243}$, GFP-FtsN$^{1–105}$, or GFP-FtsN$^{1–90}$ was sufficient to support division in either FtsN-depleted or Δ*ftsN* cells (Fig. 3), but production of GFP-FtsN$^{1–81}$ was not. Western analyses indicated that the latter fusion was not any less stable than the former (see Fig. S1A in the supplemental material). These results confirmed that most of the periplasmic portion of FtsN is dispensable and indicated that residues in the residue 81 to 90 interval are required for its essential function(s).

To assess if small periplasmic peptides covering this region are also sufficient, we next tested fusions to ^{TT}GFP, which were directed to the periplasm via the twin-arginine transporter (Tat) by use of the TorA signal peptide (Fig. 1). This showed that production of ^{TT}GFP-FtsN$^{71–105}$ from pMG14 was indeed sufficient to support division of both FtsN-depleted (CH31) and Δ*ftsN* (CH34) cells (Fig. 1 and 3D). As might be expected, this periplasmic fusion supported cell division less efficiently

TABLE 3. Division phenotypes of SPOR protein mutants[a]

Strain[b]	Genotype	Avg cell length (SD) (μm)	Avg unit length (μm)	% Cells with indicated no. of constrictions				
				0	1	2	3	>3
TB28	WT	4.6 (1.2)	3.5	69.7	30.3			
BL38	*damX*	4.7 (1.1)	3.5	64.3	35.7			
MG14	*dedD*	8.4 (4.3)	5.4	53.0	40.5	4.8	1.7	
FB70	*rlpA*	4.3 (1.1)	3.2	67.9	32.1			
BL40	*damX dedD*	16.6 (12.0)	8.4	38.6	37.7	16.1	5.4	2.2
BL41	*dedD rlpA*	8.3 (2.9)	5.4	50.9	45.4	3.7		
BL48	*damX dedD rlpA*	20.4 (13.0)	8.8	24.0	41.8	20.4	8.9	4.9
TB77	*ftsN*^{slm117}	13.3 (6.9)	6.4	29.9	53.4	10.3	6.0	0.4
BL43	*ftsN*^{slm117} *damX*	26.4 (16.2)	12.2	27.5	41.4	21.6	7.7	1.8
MG19[c]	*ftsN*^{slm117} *dedD*							
BL44	*ftsN*^{slm117} *rlpA*	9.1 (4.2)	6.00	53.5	42.5	2.5	1.0	0.5
BL45	*ftsN*^{slm117} *damX rlpA*	26.2 (14.2)	11.7	22.5	42.5	27.0	6.5	1.5

[a] Cell length refers to the total distance between the ends of a cell or chain. Unit length refers to the distance between ends of an unconstricted cell, the distance between a constriction and the nearest cell end, or the distance between consecutive constrictions. At least 200 cell or cell chains were analyzed in each case.
[b] Cells were chemically fixed after growth for about five generations in LB to an optical density at 600 nm of 0.5 to 0.6 and imaged with DIC optics.
[c] Not viable unless FtsN or DedD supplied ectopically (see text).

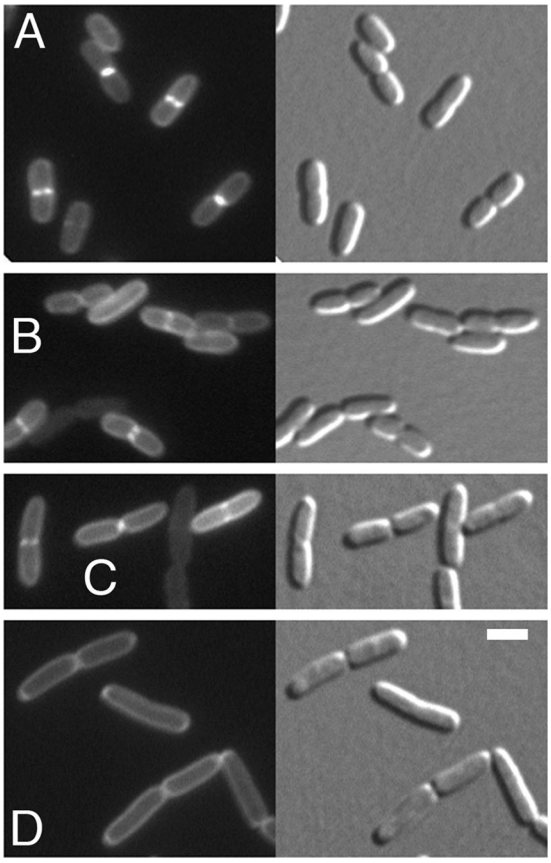

FIG. 3. Functionality and localization of fusions in Δ*ftsN* cells. Shown are fluorescence (left) and corresponding DIC (right) images of live cells of strain CH34 (Δ*ftsN*) harboring pCH201 (P_{lac}::*gfp-ftsN*) (A), pCH354 (P_{lac}::*gfp-ftsN*$^{1–243}$) (B), pMG47 (P_{lac}::*gfp-ftsN*$^{1–90}$) (C), or pMG14 (P_{lac}::^{TT}*gfp-ftsN*$^{71–105}$) (D). Cells were grown to an optical density at 600 nm of 0.6 to 0.8 in M9-glucose medium supplemented with 5 μM (A to C) or 50 μM (D) IPTG. Note the poor accumulation of fluorescence at constriction sites in panels B to D. Bar, 2 μm.

than the functional transmembrane GFP-FtsN variants we tested. Thus, whereas Δ*ftsN* cells carrying pCH201 (P_{lac}::*gfp-ftsN*), pCH354 (P_{lac}::*gfp-ftsN*$^{1–243}$), pMG12 (P_{lac}::*gfp-ftsN*$^{1–105}$), or pMG47 (P_{lac}::*gfp-ftsN*$^{1–90}$) already attained a WT division phenotype in the presence of 5 μM IPTG, those carrying pMG14 (P_{lac}::^{TT}*gfp-ftsN*$^{71–105}$) required at least 50 μM to do so. Western analyses indicated that the periplasmic (processed) form of ^{TT}GFP-FtsN$^{71–105}$ reached a level that was about 25-fold higher than that of the transmembrane fusions under these conditions (see Fig. S1 in the supplemental material).

Expression of ^{TT}GFP-FtsN$^{71–90}$ from pMG50 failed to correct division at any concentration of inducer. This was unexpected, as the transmembrane GFP-FtsN$^{1–90}$ fusion encoded by pMG47 was fully capable of compensating for a complete lack of native FtsN (Fig. 1 and 3C). Western analyses suggested that the ^{TT}GFP-FtsN$^{71–90}$ fusion was not any less stable than ^{TT}GFP-FtsN$^{71–105}$ (see Fig. S1B, lanes 3 and 4, in the supplemental material), so it is possible that FtsN function becomes dependent on residues in the 1 to 70 interval when residues in the 91 to 105 interval are lacking.

In any event, these results showed that the essential function of FtsN can be carried out by a surprisingly small periplasmic portion of the protein. This essential domain (^{E}FtsN) comprises 35 residues (FtsN$^{71–105}$) at most and likely includes most of the residues thought to form helix H2 (~FtsN$^{80–93}$) (60). Those corresponding to H1 (~FtsN$^{62–67}$) and H3 (~FtsN$^{117–123}$), however, as well as the rest of the protein are dispensable for FtsN′s essential activity in cell division.

The SPOR domain of FtsN (^{S}FtsN) is an important septal targeting determinant. The cytoplasmic portion and most of the transmembrane helix of FtsN (FtsN$^{1–45}$) can be replaced without abrogating its ability to localize to constriction sites, suggesting that a septal localization determinant resides in its periplasmic portion (1, 12).

As the small periplasmic ^{E}FtsN domain is sufficient to support division, it is also a good candidate for directing FtsN to the SR. However, we failed to detect any specific accumulation of the functional ^{TT}GFP-^{E}FtsN fusion at the division sites of CH34/pMG14 (Δ*ftsN*/P_{lac}::^{TT}*gfp-ftsN*$^{71–105}$) cells. This was so at the minimal concentration of IPTG needed to stimulate a close-to-normal division frequency (50 μM), as well as at lower concentrations of inducer, at which cells became progressively more filamentous (Fig. 3D and data not shown). Rather, the fusion appeared dispersed throughout the periplasm, and similar fluorescent halos were seen when ^{TT}GFP-^{E}FtsN was expressed in WT or *ftsN*^{slm117} cells, even at very low levels (Fig. 2D and data not shown). Western analyses indicated that the ^{TT}GFP-^{E}FtsN fusion was not completely stable (see Fig. S1B, lane 3, in the supplemental material), raising the possibility that the dispersed periplasmic fluorescence was a consequence of proteolytic release of an intact GFP moiety. Although this caveat is difficult to rule out, the ^{TT}GFP-^{E}FtsN fusion appeared no less stable than another ^{TT}GFP-FtsN fusion that did localize to division sites (^{TT}GFP-^{S}FtsN [see below]), rendering this possibility unlikely. Taken together, these results suggest that ^{E}FtsN by itself has little, if any, specific affinity for the division apparatus.

To more precisely identify the domain(s) of FtsN responsible for targeting to the septal ring, we inspected live TB28 (WT) cells and, where possible, CH34 (Δ*ftsN*) cells producing various other GFP fusions by fluorescence microscopy. Fusions were qualitatively judged to have accumulated at (prospective) constriction sites only if fluorescence intensity at the site appeared markedly higher than at the remainder of the cell's periphery. For comparison, we also scored the localization patterns of ZipA$^{1–183}$-GFP, a transmembrane ZipA derivative that lacks an FtsZ-binding domain and no longer accumulates at SRs. As seen before (36), this fusion appeared evenly distributed along the membrane in the large majority (96%; n = 381) of TB28/pCH178 (WT/P_{lac}::*zipA*$^{1–183}$-*gfp*) cells (Fig. 4B; Table 4). The remaining cells (n = 14) were scored as showing a notably higher signal at a cell constriction site than elsewhere. Although this could reflect some remaining affinity of the ZipA$^{1–183}$-GFP fusion for the division apparatus in some cells, it more likely reflects inaccuracies in image aquisition and/or interpretation.

When produced as the sole FtsN derivative in CH34 (Δ*ftsN*) cells, the fusion of GFP to full-length FtsN (GFP-FtsN) showed a clear ring-like accumulation at midcell in 42% of cells in an exponentially growing culture (Fig. 3A; Table 4). In

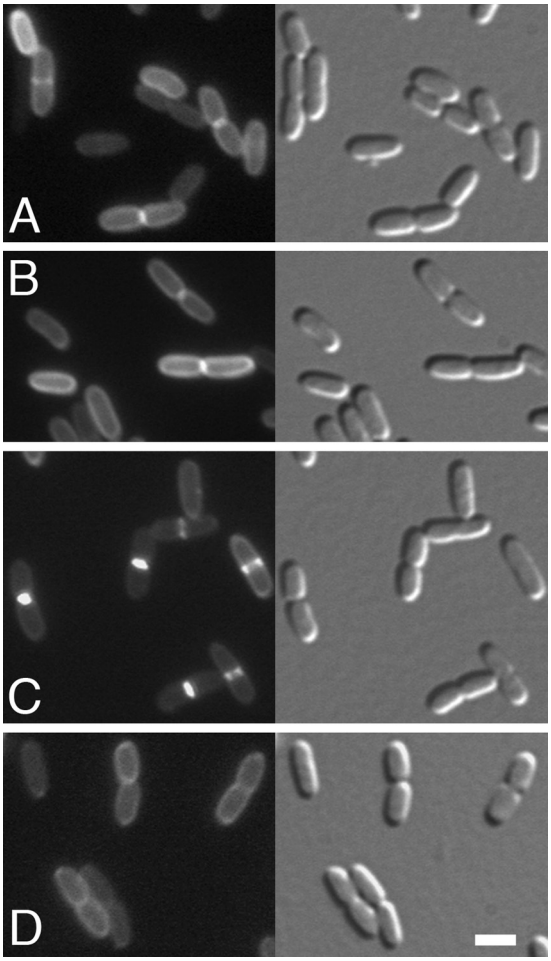

FIG. 4. Septal localization of ^{TT}GFP-^{S}FtsN. Shown are fluorescence (left) and corresponding DIC (right) images of live cells of strain TB28 (WT) harboring pMG13 (P_{lac}::*gfp-ftsN*$^{1–81}$) (A), pCH178 (P_{lac}::*zipA*$^{1–183}$-*gfp*) (B), pMG4 (P_{lac}::^{TT}*gfp-ftsN*$^{241–319}$) (C), or pMG5 (P_{lac}::^{TT}*gfp-ftsN*$^{281–319}$) (D). Cells were grown to an optical density at 600 nm of 0.6 to 0.8 in M9-glucose medium supplemented with 5 μM IPTG. Note the sharp accumulation of ^{TT}GFP-^{S}FtsN at constriction sites in panel C. Bar, 2 μm.

a small subpopulation of these (5%), a ring was present in cells that did not yet show a visible sign of constriction when observed with differential interference contrast (DIC) optics. In all other cases, the ring coincided with readily detectible constrictions. Not all constricting cells were scored as showing a clear ring, and this was particularly so with deeply constricted cells. Although the fusion was always present at constriction sites, many of these cells showed an additional fluorescent signal along the entire membrane that was too high relative to the "ring" at the constiction site to confidently classify the latter as an obvious accumulation of the fusion.

The GFP-FtsN$^{1–243}$ fusion lacks the SPOR domain, and GFP-FtsN$^{1–90}$ additionally lacks the linker region and H3 (Fig. 1). Even though these fusions were fully capable of supporting division when produced in CH34 (Δ*ftsN*) cells (Fig. 1 and 3) and did not appear any less stable than GFP-FtsN$^{1–319}$ (see Fig. S1A in the supplemental material), they both showed an obvious and similar localization defect (Fig. 3B and C and Table 4). Either fusion appeared to accumulate in rings in only a small subpopulation of cells (~15%), and none of these was at the early stage of constriction, when cell envelope invagination is still difficult to detect by DIC. The fusions appeared homogenously distributed along the membrane in the remaining cells, which, in addition to all unconstricted cells, included the majority (~75%) of constricted individuals. These results indicated that the SPOR domain is required for efficient accumulation of FtsN at constriction sites.

To assess if this domain (^{S}FtsN) is also sufficient for septal targeting, we examined WT cells producing ^{TT}GFP-^{S}FtsN, a periplasmic fusion containing just this domain and encoded on pMG4 (P_{lac}::^{TT}*gfp-ftsN*$^{241–319}$) (Fig. 1). Indeed, this fusion localized sharply at sites of constriction (Fig. 4C). A clear medial ring was observed in 60% of the total population, including 5% of unconstricted and in almost all (95%) constricted cells (Table 4). In contrast, cells expressing a fusion to an incomplete SPOR domain (^{TT}GFP-FtsN$^{281–319}$) (Fig. 1) only showed fluorescent halos (Fig. 4D). Little, if any, of the intact periplasmic form of this fusion could be detected by immunoblotting, suggesting it was rapidly degraded (see Fig. S2, lane 5, in the supplemental material).

We conclude that the SPOR domain of FtsN (^{S}FtsN) is an important septal localization determinant. Even though the SPOR-less GFP-FtsN$^{1–243}$ and GFP-FtsN$^{1–90}$ fusions localized poorly relative to GFP-FtsN and GFP-^{S}FtsN, they did appear to accumulate to some degree at the constriction site in about one-fifth of constricting CH34 cells (Table 4). This suggests that the first 90 residues of FtsN include an additional septal localization determinant(s) but that any such determinant is significantly weaker than ^{S}FtsN.

TABLE 4. Accumulation of fusions in rings

Strain[a]	Fusion	Total no. of cells	% Cells with:		% Constrictions with ring[b]			% Rings without constriction
			Constriction	Ring	All	Shallow	Deep	
CH34/pCH201	GFP-FtsN	345	58	42	69	86	41	5
CH34/pCH354	GFP-FtsN$^{1–243}$	302	68	15	22	26	15	0
CH34/pMG47	GFP-FtsN$^{1–90}$	207	64	16	25	34	14	0
TB28/pMG13	GFP-FtsN$^{1–81}$	248	42	6	13	13	14	0
TB28/pMG4	GFP-FtsN$^{241–319}$	208	60	60	95	100	90	5
TB28/pCH178	ZipA$^{1–183}$-GFP	381	47	4	8	8	8	0

[a] Cells were imaged live after growth for about four generations in M9-glucose medium with 5 μM IPTG to an optical density at 600 nm of 0.65 to 070.
[b] Each constriction in the cell population visible by DIC (all) was classified as either shallow (formation of polar caps less than halfway completed) or deep (all others); in addition, whether the constriction was accompanied by a clear fluorescent ring structure was determined.

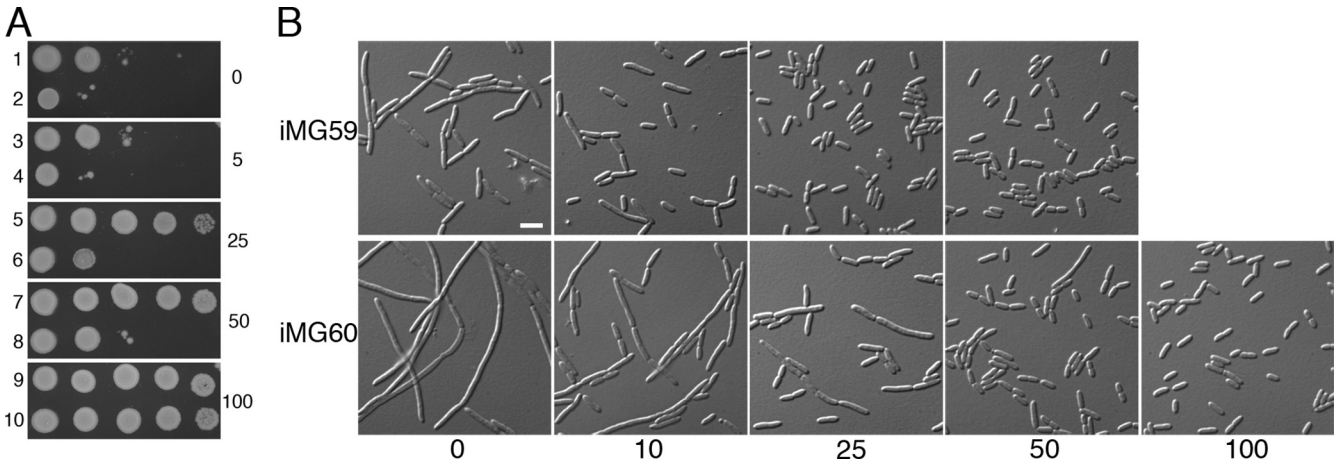

FIG. 5. Diminished efficiency of SPOR-less FtsN in supporting cell division. (A) Spot titer analysis of CH34(iMG59) [Δ*ftsN*(P_{lac}::*gfp-ftsN*)] (uneven rows) and CH34(iMG60) [Δ*ftsN*(P_{lac}::*gfp-ftsN*$^{1–243}$)] (even rows). Cells were grown overnight in LB with 50 μM IPTG, washed, and resuspended in LB to an optical density at 600 nm of 4×10^{-1}, 4×10^{-2}, 4×10^{-3}, 4×10^{-4}, and 4×10^{-5} (from left to right). Five microliters of each dilution was then spotted on LB agar containing 0, 5, 25, 50, or 100 μM IPTG, as indicated, and plates were incubated at 30°C for 16 h. (B) Division phenotypes in liquid minimal medium. Cells were grown in M9-glucose medium with 25 μM [strain CH34(iMG59); upper images] or 100 μM [strain CH34(iMG60); lower images] IPTG. Cultures were then diluted 200-fold in M9-glucose with 0, 10, 25, 50, or 100 μM IPTG, as indicated, grown to an optical density at 600 nm of 0.33 to 0.43, and imaged. Bar, 4 μm.

ftsN^{slm117} cells suffer a partial deficiency in ^{E}FtsN activity. As in Δ*ftsN* cells (see above), production of ^{TT}GFP-^{E}FtsN was sufficient to restore a normal division frequency in TB77 (*ftsN*^{slm117}) cells, even though the fusion showed no sign of specific accumulation at constriction sites (Fig. 2C and D). Conversely, the ^{TT}GFP-^{S}FtsN fusion failed to suppress the chaining phenotype of TB77, even though it accumulated sharply at constriction sites in these chains (Fig. 2F).

These results imply that the chaining phenotype of *ftsN*^{slm117} cells is caused by a partial deficiency in ^{E}FtsN activity, which could be due to instability of the FtsN^{slm117} peptide, a failure to concentrate this SPOR-less peptide at the presumed site of ^{E}FtsN action (the SR), or a combination of both. The inference that a reduction of ^{E}FtsN activity at the SR leads to a prolonged constriction period and cell chaining is consistent with the phenotype of cells with suboptimal FtsN levels (Fig. 5B) (see below).

The sharp localization of ^{TT}GFP-^{S}FtsN in TB77 (*ftsN*^{slm117}) cells, furthermore, ruled out the possibility that the fusion accumulated at constriction sites via SPOR-SPOR interactions with native FtsN.

^{S}FtsN contributes to the efficacy of ^{E}FtsN. The results above suggested that the SPOR domain of FtsN aids cell division by helping to concentrate ^{E}FtsN at its site of action. If so, a poorly localizing SPOR-less FtsN derivative, such as GFP-FtsN$^{1–243}$, would be expected to be less effective in restoring cell division to Δ*ftsN* cells than full-length GFP-FtsN. In order to assess this with some accuracy, we used Δ*ftsN* strains in which the GFP-FtsN and GFP-FtsN$^{1–243}$ fusions were encoded by single-copy CRIM constructs that had been integrated at the chromosomal *att*HK022 site. These strains afforded better control over the production levels of the fusions than the corresponding strains encoding the fusions on multicopy plasmids described above. In Fig. 5A, cells of strains CH34(iMG59) [Δ*ftsN*(P_{lac}::*gfp-ftsN*)] and CH34(iMG60) [Δ*ftsN*(P_{lac}::*gfp-ftsN*$^{1–243}$)] were subjected to spot titer analyses on LB agar supplemented with various concentrations of IPTG. This showed that Δ*ftsN* cells encoding the SPOR-less fusion indeed required a significantly higher concentration of inducer for good growth (100 μM) than ones rescued by the fusion to native FtsN (25 μM). The division phenotypes of cells growing in liquid M9-glucose medium were consistent with this result, although the division phenotypes of both strains were less severe than on solid medium. In the absence of inducer, most CH34(iMG59) cells already grew as short chains and they resembled WT cells at 25 μM IPTG and above, suggesting that little *gfp-ftsN* expression is needed to support cell division under these conditions (Fig. 5B, upper row). In contrast, most CH34(iMG60) cells formed long filaments with few constrictions in the absence of IPTG. At a 25 μM concentration of inducer, they roughly resembled the chains of CH34(iMG59) seen with no inducer, and they required 100 μM or more to resemble WT cells (Fig. 5B, lower row). Western analyses indicated that these differences were not due to significant differences in the stability of the fusions and that cells required about fourfold more of the SPOR-less GFP-FtsN$^{1–243}$ fusion than GFP-FtsN in order to divide normally (see Fig. S3 in the supplemental material).

^{E}FtsN-dependent targeting of ^{S}FtsN to constriction sites. While cells that lack ^{E}FtsN fail to constrict (11), ^{S}FtsN (or full-length FtsN) appeared to accumulate at the SR only at or after the onset of constriction (Table 4). Hence, septal localization of ^{S}FtsN appeared to depend on the essential activity of ^{E}FtsN. As in the context of the native protein septal localization of ^{S}FtsN will cause ^{E}FtsN to become concentrated at constriction sites as well, this predicts that FtsN accumulates at the SR by an unusual self-enhancing mechanism that requires both domains. To assess this scenario more directly, we studied the localization of ^{S}FtsN in the ^{E}FtsN depletion strain CH34/pMG20/pMG4 (Δ*ftsN*/P_{BAD}::^{TT}*bfp-ftsN*$^{71–105}$/P_{lac}::^{TT}*gfp-ftsN*$^{241–319}$) in which production of a fusion of the essential domain to Tat-targeted blue fluorescent protein (^{TT}BFP-^{E}FtsN) can be modulated with arabinose and that of ^{TT}GFP-^{S}FtsN with

IPTG. In the presence of both inducers, cells appeared to divide normally, and ^{TT}GFP-^{S}FtsN accumulated at each constriction site (Fig. 6B). In the absence of arabinose (^{E}FtsN^{-}), however, ^{TT}GFP-^{S}FtsN did not form regularly spaced rings, as might be expected if ^{S}FtsN could target SRs independently of ^{E}FtsN, but accumulated in rings only at rare constrictions still remaining in some of the filaments (Fig. 6C and data not shown). Western analyses indicated that the failure of ^{TT}GFP-^{S}FtsN to form rings in the ^{E}FtsN-depleted filaments was not due to excessive degradation of the fusion (see Fig. S2, lanes 3 and 4, in the supplemental material). We conclude that ^{S}FtsN targeting to constriction sites normally indeed depends on the presence of ^{E}FtsN.

^{E}FtsN-independent targeting of ^{S}FtsN. Two scenarios might explain the ^{E}FtsN-dependent accumulation of ^{S}FtsN at SRs. The first is that ^{S}FtsN can interact directly with ^{E}FtsN and that the latter acts as a pilot for the former. We considered this unlikely, because all GFP fusions that lacked ^{S}FtsN, especially ^{TT}GFP-^{E}FtsN, localized poorly, if at all (Fig. 1; Table 4). The second is that, even though ^{E}FtsN by itself fails to localize, it can still stimulate cell constriction when its concentration in the periplasm is sufficiently high, and ^{S}FtsN is attracted to some other feature of the constricting SR. The recent discovery that a mutant FtsA protein (FtsA^{E124A}) allows cells to grow and divide in the complete absence of FtsN (5) provided us with a means to conclusively rule out the first senario.

To this end, we first replaced *ftsA* on the chromosome of strain TB28 with *ftsA*^{E124A} and then introduced the Δ*ftsN* (*ftsN*<>*aph*) knockout lesion by P1-mediated transduction. While cells of the BL18 (*ftsA*^{E124A}) recipient strain divided at a normal frequency as expected (5), the resultant *ftsA*^{E124A} Δ*ftsN* transductant cells were very filamentous and barely viable (data not shown). The viability of transductants improved significantly, however, when recipients carried additional copies of the *ftsA*^{E124A} allele, such as on plasmid pBL12. Even then, division was not completely normal, as cells of the resulting strain, BL20/pBL12 (Δ*ftsN ftsA*^{E124A}/*ftsA*^{E124A}) displayed a chaining phenotype not unlike that of TB77 (*ftsN*^{slm117}) (Fig. 6D and E).

We next compared the localization patterns of periplasmic ^{TT}GFP and ^{TT}GFP-^{S}FtsN in BL20/pBL12 derivatives that carried a single copy of pBL5 (P_{lac}::^{TT}*gfp*) or pBL6 (P_{lac}::^{TT}*gfp-ftsN*$^{241–319}$) integrated at *att*HK022. Expression of unfused ^{TT}GFP in strain BL20(iBL5)/pBL12 resulted in an homogenous fluorescent halo around each cell without obvious ring-like accumulations at constriction sites (Fig. 6E), suggesting that chaining was due to slow constriction rather than to any defect that would cause a grossly expanded intermembrane distance at sites of constriction. In contrast, ^{TT}GFP-^{S}FtsN accumulated at each constriction site of BL20(iBL6)/pBL12 cells (Fig. 6D). We conclude that ^{S}FtsN is readily able to recognize these sites in the complete absence of any other domain of FtsN, including ^{E}FtsN.

Targeting of ^{S}FtsN is dependent on PBP3 (FtsI) activity. Given that recruitment of ^{S}FtsN to division sites appeared to depend on the onset of the constriction phase of the fission process (Fig. 6C; Table 4) and that the SPOR domains of both *E. coli* FtsN (55) and *B. subtilis* CwlC (44) have an affinity for murein, it is reasonable to suppose that the feature of constric-

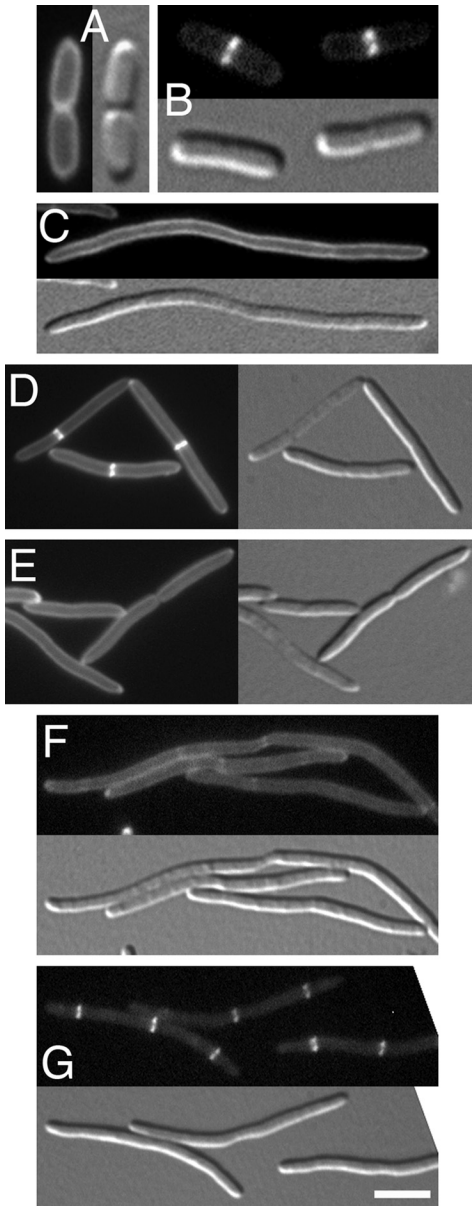

FIG. 6. Localization of ^{TT}GFP-^{S}FtsN at constriction sites depends on ^{E}FtsN and PBP3 activities. (A to C) ^{E}FtsN-dependent localization of ^{S}FtsN. Cells of ^{E}FtsN depletion strain CH34/pMG20 (Δ*ftsN*/P_{BAD}::^{TT}*bfp-ftsN*$^{71–105}$) harboring pTB6 (P_{lac}::^{TT}*gfp*) (A) or pMG4 (P_{lac}::^{TT}*gfp-ftsN*$^{241–319}$) (B and C) were grown to an optical density at 600 nm of 0.6 to 0.7 in M9-maltose supplemented with 5 μM IPTG and 0.1% of either arabinose (A and B) or glucose (C). Note the absence of fluorescent ^{TT}GFP-^{S}FtsN rings in the ^{E}FtsN-depleted filament in panel C. (D and E) In contrast to unfused ^{TT}GFP (E), ^{TT}GFP-^{S}FtsN (D) accumulates at constriction sites of Δ*ftsN* cells that manage to divide in the complete absence of ^{E}FtsN, due to production of the FtsA^{E124A} protein. Strains BL20(iBL6)/pBL12 [Δ*ftsN ftsA*^{E124A} (P_{lac}::^{TT}*gfp-ftsN*$^{241–319}$)/*ftsA*^{E124A}] (D) and BL20(iBL5)/pBL12 [Δ*ftsN ftsA*^{E124A} (P_{lac}::^{TT}*gfp*)/*ftsA*^{E124A}] (E) were grown to an optical density at 600 nm of 0.3 in M9-maltose supplemented with 25 μM IPTG. (F and G) Unlike ZipA (G), ^{S}FtsN (F) fails to accumulate in rings in cephalexin-treated cells. Overnight cultures of TB28(iBL48) [WT(P_{lac}::*zipA-gfp*)] and TB28(iBL50) [WT(P_{lac}::^{TT}*gfp-ftsN*$^{241–319}$)] were diluted 100-fold into M9-maltose with 10 μM IPTG and incubated for 2 h. Cephalexin was added to 15 μg/ml, and growth was continued to an optical density at 600 nm of 0.5. Fluorescence and corresponding DIC images of live cells are shown in each case. Bar, 2 μm (A and B) or 4 μm (C to G).

tion sites that is recognized by ^{S}FtsN includes some form of septal murein.

To test this idea further, we monitored localization of ^{TT}GFP-^{S}FtsN after treatment of cells with cephalexin, a β-lactam that specifically interferes with the murein transpeptidase activity of PBP3 (FtsI), which is specifically required for the synthesis of septal murein during cell constriction (56). As illustrated in Fig. 6F, ^{TT}GFP-^{S}FtsN localized throughout the periplasm in cephalexin-treated filaments of TB28(iBL50) [WT(P_{lac}::^{TT}*gfp-ftsN*$^{241–319}$)] cells, save for some very weak accumulations at some of the remaining constrictions. (Note that the integrative plasmid pBL50 is identical to pBL6, except that *bla* has been replaced with *cat.*) The failure of ^{TT}GFP-^{S}FtsN to accumulate in rings under these conditions was not due to excessive degradation of the fusion (see Fig. S4, lanes 2 and 3, in the supplemental material). In contrast, and as expected (30, 31), a ZipA-GFP fusion accumulated in regularly spaced rings in cephalexin-treated TB28(iBL48) [WT(P_{lac}::*zipA-gfp*)] filaments (Fig. 6G).

Targeting of ^{S}FtsN is dependent on murein amidase activity. The purified periplasmic domain of FtsN (FtsN$^{58–318}$) was previously found to preferentially bind the longest (>25 disaccharide units) glycan strands that remained upon amidase treatment of purified sacculi and to bind poorly to sacculi from cells that were deficient in murein amidase activities (55). This suggested that the septal localization of ^{S}FtsN might be impaired in amidase-deficient cells as well, and we tested this by using a set of isogenic strains lacking one, two, or all three of the *amiA*, *-B*, and *-C* genes.

^{TT}GFP-^{S}FtsN still accumulated sharply at constriction sites in cells of strains BL25 (Δ*amiA*), BL7 (Δ*amiB*), and BL9 (Δ*amiC*), as well as in the (relatively short) cell chains formed by strains BL10 (Δ*amiB* Δ*amiC*) and BL11 (Δ*amiA* Δ*amiC*) (Fig. 7A and data not shown), indicating that none of the amidases is specifically required for accumulation of ^{S}FtsN at septa. In the long cell chains formed by the triple knockout strain BL12 (Δ*amiA* Δ*amiB* Δ*amiC*), however, the localization pattern of ^{TT}GFP-^{S}FtsN (Fig. 7C) closely resembled that of unfused ^{TT}GFP (Fig. 7D). Thus, fluorescence appeared throughout the periplasm, although some weak septal accumulations along the cell chains were apparent as well. As the latter were similarly apparent with the ^{TT}GFP control, we assume these reflected an increased intermembrane distance at such sites. Western analyses indicated that the lack of specific accumulation at septa was not due to excessive processing of ^{TT}GFP-^{S}FtsN in strain BL12 (see Fig. S2, lane 2, in the supplemental material).

We conclude that efficient targeting of ^{S}FtsN to sites of constriction indeed requires the activity of at least one of the three periplasmic murein amidases in *E. coli*.

DedD is a new septal ring component that contributes to the cell constriction process and is essential in *ftsN*^{Slm117} cells. In addition to FtsN, three *E. coli* proteins with unknown functions (DamX, DedD, and RlpA) are predicted to also contain a C-terminal SPOR domain that resides in the periplasm.

Among these, DedD (named for *d*ownstream *E. coli* DNA *D* [47]) drew our particular attention because we also recovered a *dedD*::EzTn transposon insertion allele in a genetic screen for new cell shape/division mutants in a parallel project (4). This allele caused a distinct division phenotype that was recapitulated in strains in which *dedD* had been removed by targeted deletion (Fig. 8A). Thus, both *dedD*::EzTn and Δ*dedD* cells showed a chaining phenotype that was reminiscent of that of *ftsN*^{Slm117} cells, but milder (Fig. 8B and D, Table 3, and data not shown). Cell chaining was fully suppressible by expression of *dedD* or *gfp-dedD* from plasmid or lysogenic phage constructs (Fig. 8C and data not shown), implying that the phenotype was not due to polar effects of the *dedD* lesions and that the GFP-DedD fusion retained function (Fig. 8C and data not shown). Moreover, GFP-DedD accumulated in septal rings. Localization was especially sharp in constricting cells, although weaker accumulations were apparent in some preconstricting cells as well (Fig. 8C).

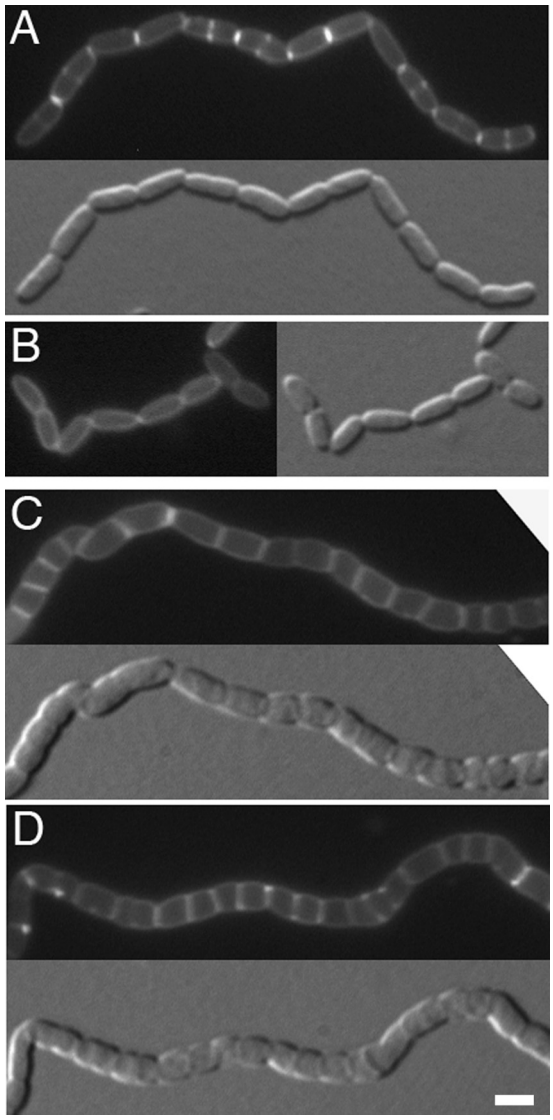

FIG. 7. Localization of ^{TT}GFP-^{S}FtsN and ^{TT}GFP in murein amidase mutants. Shown are fluorescence and corresponding DIC images of live cells of strains BL11 (*amiA amiC*) (A and B) and BL12 (*amiA amiB amiC*) (C and D) harboring pMG4 (P_{lac}::^{TT}*gfp-ftsN*$^{241–319}$) (A and C) or pTB6 (P_{lac}::^{TT}*gfp*) (B and D). Cells were grown to an optical density at 600 nm of 0.5 to 0.6 in M9-glucose medium supplemented with 2.5 μM IPTG. Note the sharp accumulation of ^{TT}GFP-^{S}FtsN at constriction sites in panel A. Bar, 2 μm.

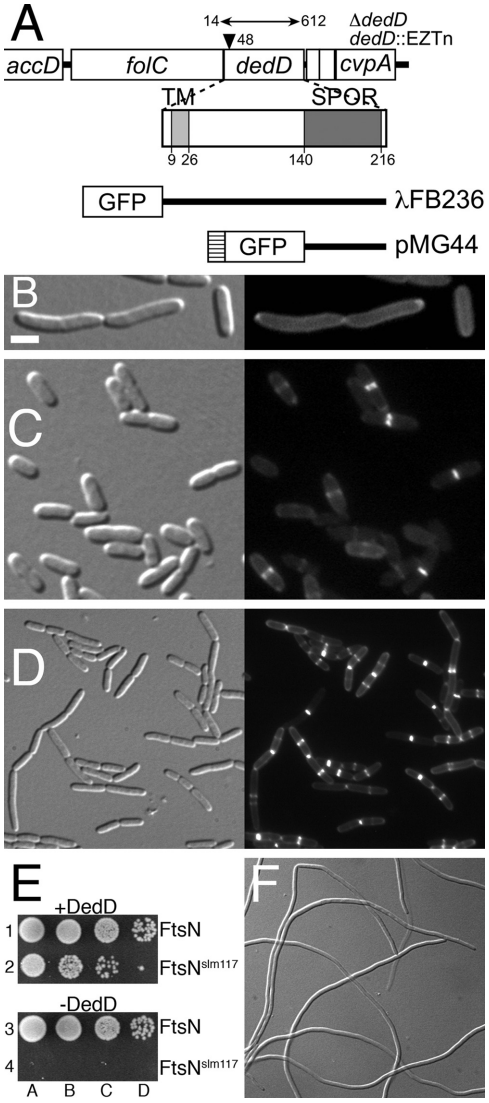

FIG. 8. DedD is a new septal ring protein that is required for division of *ftsN*^{slm117} cells. (A) *E. coli dedD* locus, DedD domains, and fusion constructs. Shown are the EZTnKan-2 insertion site in *dedD*::EZTn strains and the deletion replacements in *dedD*<>*cat* and *dedD*<>*frt* (Δ*dedD*) strains. Numbers refer to the site of insertion (black triangle) or to the base pairs that were replaced (doubleheaded arrow), counting from the start of *dedD*. The domain structure of DedD is illustrated below the *dedD* gene. Indicated are the transmembrane domain (TM; light gray) and the C-terminal periplasmic SPOR domain (^{S}DedD; dark gray). Inserts present on lysogenic phage λFB236 (P$_{lac}$::*gfp-dedD*) or plasmid pMG44 (P$_{lac}$::^{TT}*gfp-dedD*$^{140–220}$) are indicated. (B to D) Chaining of Δ*dedD* cells (B and D) and septal localization of GFP-DedD (C) and ^{TT}GFP-^{S}DedD (D). Shown are DIC and corresponding fluorescence images of live cells of strain MG14 (Δ*dedD*) harboring plasmid pMG44 (P$_{lac}$::^{TT}*gfp-dedD*$^{140–220}$) (D) or lysogenic for either λTB6 (P$_{lac}$::^{TT}*gfp*) (B) or λFB236 (P$_{lac}$::*gfp-dedD*) (C). Cells were grown in M9-glucose with 5 μM (D), 25 μM (C), or 50 μM (B) IPTG to an optical density at 600 nm of 0.6 to 0.7. Note the correction of cell chaining in panel C and the accumulation of fluorescence at division sites in both panels C and D. (E and F) Lethal division block in *ftsN*^{slm117} cells lacking DedD. Depletion of DedD from *ftsN*^{slm117} cells is lethal (E). Strains MG14(λFB236) [Δ*dedD*(P$_{lac}$::*gfp-dedD*)] (rows 1 and 3) and MG19(λFB236) [Δ*dedD ftsN*^{slm117}(P$_{lac}$::*gfp-dedD*)] (rows 2 and 4) were grown overnight in LB with 100 μM IPTG. Culures were diluted 10^3-, 10^4-, 10^5-, and 10^6-fold (left to right), and 5 μl was spotted on LB agar containing no (rows 3 and 4) or 100 μm (rows 1 and 2) IPTG. (F) Depletion of DedD from *ftsN*^{slm117} cells results in the formation of very long, mostly nonseptate filaments. An overnight culture of MG19(λFB236) [Δ*dedD ftsN*^{slm117}(P$_{lac}$::*gfp-dedD*)] in LB with 5 μM IPTG was diluted 100-fold into LB supplemented with 0.1% glucose and grown to an optical density at 600 nm of 0.66. Bar, 2 μm (B and C), 4 μm (D), or 8 μm (F).

To assess if the SPOR domain of DedD (DedD$^{140–220}$, ^{S}DedD) by itself was sufficient for septal localization, we monitored a ^{TT}GFP-^{S}DedD fusion containing just this domain. Indeed, the fusion localized sharply to constriction sites, although it failed to correct the chaining phenotype of Δ*dedD* cells (Fig. 8D).

Notably, while the absence of DedD in otherwise WT cells caused only mild cell chaining, it proved lethal to *ftsN*^{slm117} cells. Initial attempts to introduce Δ*dedD* in *ftsN*^{slm117} cells, or vice versa, were fruitless, indicating that the combination was synthetically lethal. To elucidate the cause of lethality, we used depletion strains in which GFP-DedD is the sole source of DedD and its production can be modulated with IPTG. Figure 8E illustrates that strain MG14(λFB236) [Δ*dedD*(P$_{lac}$::*gfp-dedD*)] grew equally well in the presence (row 1) or absence (row 3) of inducer, but that strain MG19(λFB236) [*ftsN*^{slm117}Δ*dedD*(P$_{lac}$::*gfp-dedD*)] indeed failed to propagate in its absence (row 4). Cells of the latter strain showed the typical chaining phenotype associated with *ftsN*^{slm117} in the presence of inducer (DedD^{+}) (data not shown). However, they formed very long nonseptate filaments in its absence (DedD^{-}) (Fig. 8F), implying that DedD becomes essential for cell constriction in cells that produce only the truncated form of FtsN.

We conclude that DedD is a new nonessential division protein in *E. coli* that is required for efficient cell constriction and that becomes essential in *ftsN*^{slm117} cells.

DamX and RlpA are also new septal ring components. The *damX* gene (37, 43) lies immediately upstream of that for DNA adenine methylase (*dam*) (Fig. 9A). Like FtsN and DedD, DamX is a bitopic type II membrane protein with a large periplasmic domain. Earlier insertional mutagenesis of *damX* resulted in no obvious phenotype, although overexpression of the gene led to inhibition of division, suggesting some involvement of DamX in the division process (43). To test the prediction that DamX also associates with the septal ring, we monitored cells producing fluorescent fusions to the full-length protein and to the isolated SPOR domain (DamX$^{338–428}$, ^{S}DamX) (Fig. 9A). Both YFP-DamX (Fig. 9B) and ^{TT}GFP-^{S}DamX (Fig. 9C) indeed localized sharply to division sites in WT cells, further implicating the protein in some division-associated function and showing that its SPOR also targets constriction sites autonomously.

Inspection of BL38 (Δ*damX*) cells confirmed the original observation (43) that the absence of the protein has no obvious phenotype in otherwise *wt* cells (Table 3 and data not shown). However, introduction of Δ*damX* into either *ftsN*^{slm117} or Δ*dedD* cells clearly aggravated their chaining phenotypes (Table 3). This aggravated phenotype of Δ*damX ftsN*^{slm117} or Δ*damX* Δ*dedD* double mutant cells could be suppressed to roughly that seen with *ftsN*^{slm117} or Δ*dedD* single mutants by expression of *damX* from plasmid pBL47 (P$_{lac}$::*damX*), con-

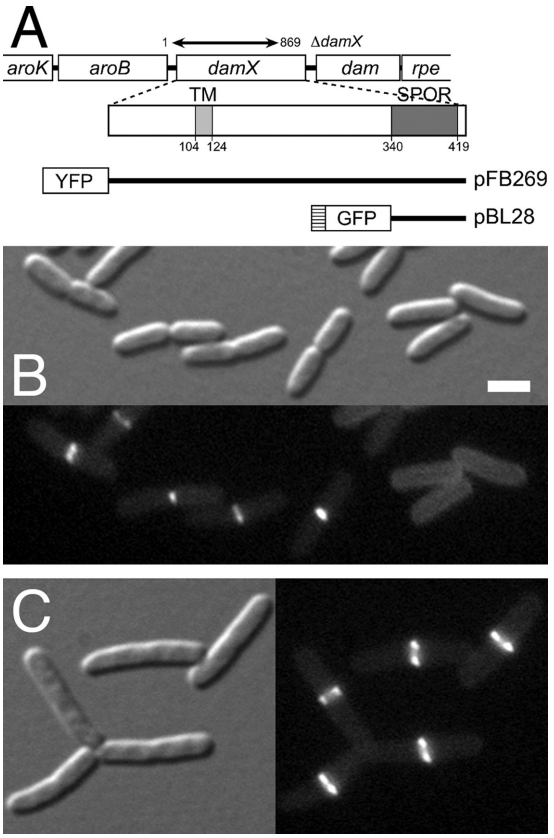

FIG. 9. DamX is also a new septal ring component. (A) *E. coli damX* locus, DamX domains, and fusion constructs. Indicated are the *damX* base pairs (doubleheaded arrow) that were replaced in *damX*<>*cat* and *damX*<>*frt* (Δ*damX*) strains, the transmembrane (TM; light gray), and the C-terminal periplasmic SPOR (^{S}DamX; dark gray) domains of DamX, and also the inserts present on plasmids pFB269 (P_{lac}::*yfp-damX*) and pBL28 (P_{lac}::^{TT}*gfp-damX*$^{338–428}$). (B) Accumulation of YFP-DamX at division sites. Cells of strain TB28/pFB269 (WT/P_{lac}::*yfp-damX*) were grown in M9-glucose with 2.5 μM IPTG to an optical density at 600 nm of 0.5. (C) Accumulation of ^{TT}GFP-^{S}DamX at division sites. Cells of strain TB28/pBL28 (WT/P_{lac}::^{TT}*gfp-damX*$^{338–428}$) were grown in LB with 5 μM IPTG to an optical density at 600 nm of 0.5. Bar, 2 μm.

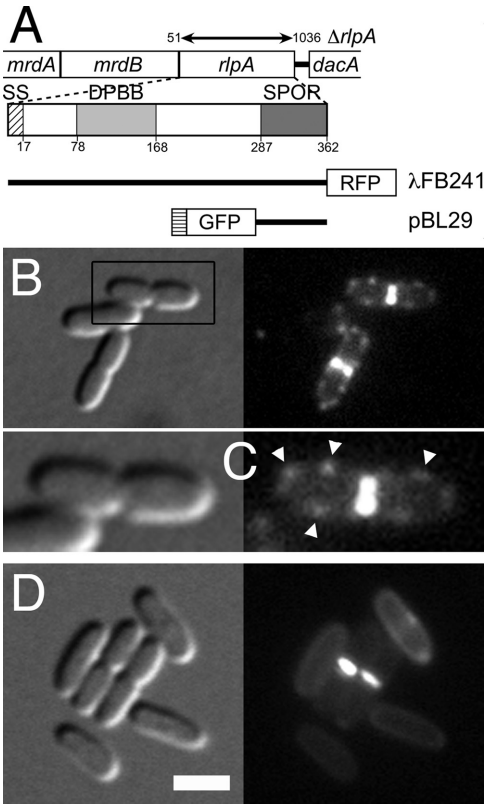

FIG. 10. Localization of RlpA. (A) *E. coli rlpA* locus, RlpA domains, and fusion constructs. Indicated are the *rlpA* base pairs (doubleheaded arrow) that were replaced in *rlpA*<>*cat* and *rlpA*<>*frt* (Δ*rlpA*) strains, the signal sequence (SS; striped), a predicted doublepsi β-barrel motif (Pfam DPBB_1; light gray), and the C-terminal SPOR domain (^{S}RlpA; dark gray) of RlpA, and also the inserts present on lysogenic phage λFB241 (P_{lac}::*rlpA-rfp*) or plasmid pBL29 (P_{lac}::^{TT}*gfp-rlpA*$^{281–362}$). (B and C) Accumulation of RlpA-RFP at division sites, as well as in foci along the cell periphery. One cell from panel B (boxed) is enlarged in panel C. Arrowheads in panel C point at nonseptal accumulations of RlpA-RFP. Cells of strain MG13(λFB241) [Δ*rlpA*(P_{lac}::*rlpA-rfp*] were grown in M9-maltose with 100 μM IPTG to an optical density at 600 nm of 0.5. (D) Accumulation of ^{TT}GFP-^{S}RlpA at division sites. Cells of strain TB28/pBL29 (WT/P_{lac}::^{TT}*gfp-rlpA*$^{281–362}$) were grown in M9-glucose with 5 μM IPTG to an optical density at 600 nm of 0.3. Note the absence of obvious nonseptal accumulations of ^{TT}GFP-^{S}RlpA. Bar, 1 μm (C) or 2 μm (B and D).

firming that aggravation of the division defects observed in the double mutants was indeed caused by the absence of DamX (data not shown). In contrast, production of YFP-DamX failed to alleviate the chaining phenotypes of the double mutants, indicating that appending YFP to its N terminus interfered with DamX function (data not shown).

We conclude that DamX is also a new division protein in *E. coli* and that the protein contributes in a nonessential manner to the constriction process when FtsN or DedD function is compromised.

RlpA is an outer membrane lipoprotein (53), setting it apart from the other three *E. coli* SPOR domain proteins, which are all type II (N-in) bitopic inner membrane species. To monitor localization of the full-length protein, we used an RlpA-RFP (RlpA-mCherry) fusion encoded on lysogenic phage λFB241 (P_{lac}::*rlpA-rfp*). To monitor that of its SPOR domain (RlpA$^{281–362}$, ^{S}RlpA), we used a Tat-targeted fusion of GFP to this domain (Fig. 10A). As shown in Fig. 10B, the RlpA-RFP fusion accumulated at constriction sites as seen above for FtsN, DamX, and DedD. Unlike the latter proteins, however, RlpA-RFP additionally accumulated in a pattern of foci, arcs, or perhaps more extended stuctures along the rest of the cell envelope in both dividing and nondividing cells (Fig. 10B and C and data not shown). This suggests that a portion of RlpA molecules is recruited to the site of division while another portion remains associated with some other structures/complexes along the cell cylinder. In contrast, and much like the other four SPOR fusions studied above, the ^{TT}GFP-^{S}RlpA fusion accumulated sharply at division sites and not in any other obvious nonhomogenous pattern (Fig. 10D). This indicates that, while ^{S}RlpA is sufficient to recognize division sites, the incorporation of full-length RlpA in the nonseptal accumulations involves other parts of the protein.

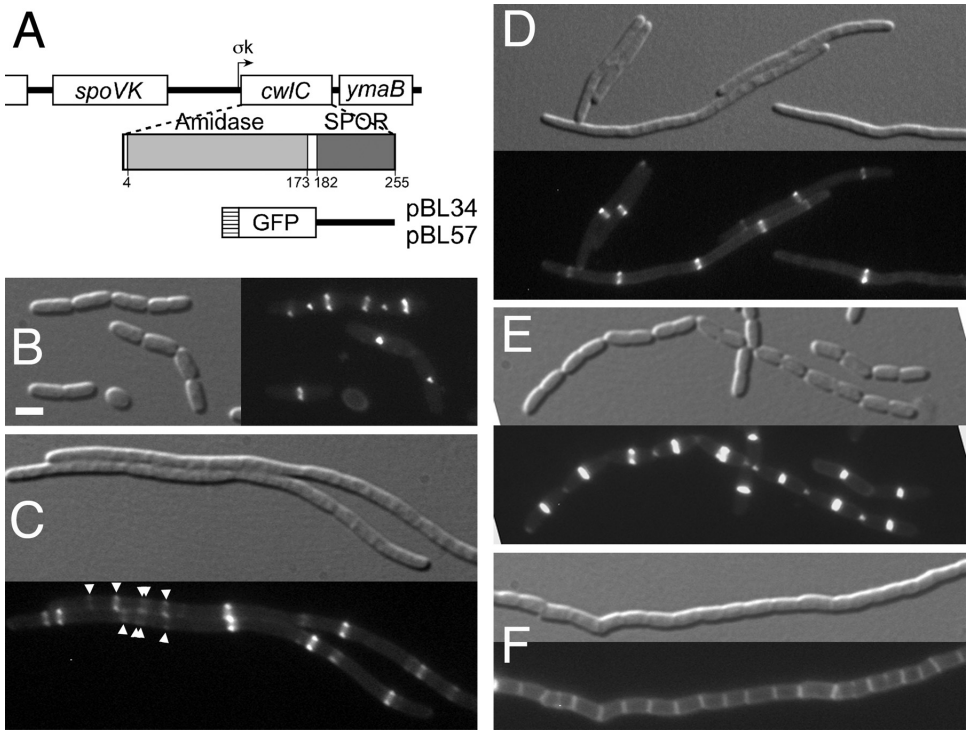

FIG. 11. Sharp accumulation of the SPOR domain of *B. subtilis* CwlC at division sites in *E. coli*. (A) *B. subtilis cwlC* locus, CwlC domains, and ^{S}CwlC fusion constructs. Indicated are the catalytic (light gray) and SPOR (^{S}CwlC; dark gray) domains of CwlC, and also the insert present on plasmids pBL34 and pBL57 (P_{lac}::^{TT}*gfp-cwlC*$^{181–255}$). The latter is an integrative CRIM construct that lacks *bla* (Table 1). (B) Cells of strain TB28/pBL34 (WT/P_{lac}::^{TT}*gfp-cwlC*$^{181–255}$) were grown in M9-glucose with 2.5 μM IPTG to an optical density at 600 nm of 0.5. Note the induction of cell chaining and the sharp localization of ^{TT}GFP-^{S}CwlC to division sites. (C) Localization of ^{TT}GFP-^{S}CwlC in ^{E}FtsN-depleted filaments. In addition to strong levels of accumulation at remaining sites of constriction, the fusion accumulated in weaker ring-like structures. Arrowheads point at multiple closely spaced dim rings present in both filaments. Strain CH34/pMG20 (Δ*ftsN*/P_{BAD}::^{TT}*bfp-ftsN*$^{71–105}$) harboring pBL34 (P_{lac}::^{TT}*gfp-cwlC*$^{181–255}$) was grown overnight in M9-maltose with 0.01% arabinose. Cells were diluted 50-fold into M9-maltose supplemented with 5 μM IPTG and 0.2% glucose, and growth was continued to an optical density at 600 nm of 0.6. (D) Localization of ^{TT}GFP-^{S}CwlC in cephalexin-treated filaments. An overnight culture of TB28(iBL57) [WT(P_{lac}::^{TT}*gfp-cwlC*$^{181–255}$)] was diluted 100-fold into M9-maltose with 5 μM IPTG and grown for 2 h. Cephalexin was added to 15 μg/ml, and growth was continued to an optical density at 600 nm of 0.5. (E and F) Localization of ^{TT}GFP-^{S}CwlC in double (E) and triple (F) amidase mutants. Strains BL11 (*amiA amiC*) and BL12 (*amiA amiB amiC*), each harboring pBL34, were grown in M9-glucose with 2.5 μM IPTG to an optical density at 600 nm of 0.5. Bar, 2 μm.

RlpA is not essential for cell viability (2, 23) and deletion of *rlpA*, by itself or when combined with Δ*damX*, Δ*dedD*, and/or *ftsN*^{slm117}, did not result in any obvious additional growth or division defects (Table 3). Thus, even though RlpA accumulates at the SR, whether it fullfills any role during the constriction process remains unclear.

Targeting of *Bacillus subtilis* ^{S}CwlC to constriction sites in *E. coli*. *Bacillus subtilis* CwlC is a murein amidase that is produced at a late stage of endospore formation, where it contributes to lysis of the mother cell compartment and release of the mature spore (39, 41, 52). In addition to an N-terminal catalytic domain, the protein contains a C-terminal SPOR domain (Fig. 11A) that has affinity for amidase-digested *B. subtilis* murein, as inferred from nuclear magnetic resonance chemical shift analyses (44, 51).

To assess if a SPOR domain from a heterologous gram-positive source has similar properties in vivo as that of the four *E. coli* proteins, we examined the localization pattern of ^{TT}GFP-^{S}CwlC, a Tat-targeted fusion containing just this domain (CwlC$^{181–255}$), in various *E. coli* strains. Interestingly, this fusion localized very sharply to constriction sites (Fig. 11B to E). In addition, expression of the fusion induced chaining of WT cells, suggesting it may compete with DamX, DedD, and/or FtsN for a septal localization target (Fig. 11B).

These results suggest that all five SPOR domains examined here recognize the same or closely related target molecules that are highly enriched at constriction sites in *E. coli*. The fact that this includes a SPOR domain from a distantly related organism suggests this may be true for such domains from many other bacterial species as well.

Localization in ^{E}FtsN-deficient cells suggests distinct properties of SPOR domains. Finally, as for ^{S}FtsN above (Fig. 5 and 6), we examined the localization patterns of the SPOR domains of CwlC, DamX, DedD, and RlpA in amidase-deficient chains and ^{E}FtsN-depleted filaments. As summarized in Table 5 and illustrated for ^{TT}GFP-^{S}CwlC in Fig. 11, all four SPOR domains behaved similarly to that of FtsN in amidase mutants. Each still localized sharply to constriction sites in chains of single or double *ami* mutants but failed to do so in chains of the triple *amiABC* mutant (Fig. 11E and F, Table 5, and data not shown).

However, we did observe distinct localization patterns in ^{E}FtsN-depleted filaments of strain CH34/pMG20. ^{S}RlpA behaved like ^{S}FtsN and appeared distributed throughout the

TABLE 5. Accumulation of SPOR domains in rings

Plasmid[a]	^{TT}GFP fusion	Accumulation of indicated SPOR domain in ring structures[b]:				
		TB28 (WT)	BL11 (Δ*amiA* Δ*amiC*)	BL12 (Δ*amiA* Δ*amiB* Δ*amiC*)	CH34/pMG20 (Δ*ftsN*/P_{BAD}::*bfp*-^{E}*ftsN*)	
					+Ara	+Glu
pBL34	^{S}CwlC	+	+	−	+	+
pBL28	^{S}DamX	+	+	−	+	+
pMG44	^{S}DedD	+	+	−	+	+
pMG4	^{S}FtsN	+	+	−	+	−
pBL29	^{S}RlpA	+	+	−	+	−

[a] Cells harboring the indicated plasmids were treated as described in the legends for Fig. 6, 7, and 11.
[b] +, the fusion accumulated in ring structures; −, the fusion was dispersed in the periplasm.

periplasm (Table 5). Western analyses indicated that this was not caused by excessive degradation of the ^{TT}GFP-^{S}RlpA fusion (see Fig. S5, lanes 7 and 8, in the supplemental material). In contrast, the other three SPOR domains still accumulated in readily discernible ring-like structures (Table 5), which are illustrated for ^{TT}GFP-^{S}CwlC in Fig. 11C. In addition to relatively strong accumulations at remaining sites of constriction, the ^{TT}GFP fusions to these three SPOR domains also formed multiple weaker rings along the length of these filaments, and the spacing between these was often quite irregular (Fig. 11C and data not shown).

The finding that septal localization of these three SPOR domains appeared significantly less sensitive to depletion of ^{E}FtsN than that of FtsN itself suggested that their localization might also be less sensitive to interference with the activity of PBP3. We tested this for ^{TT}GFP-^{S}CwlC by treatment of strain TB28(iBL57) [WT(P_{lac}::^{TT}*gfp*-^{S}*cwlC*)] with cephalexin. In contrast to ^{TT}GFP-^{S}FtsN (Fig. 6F), ^{TT}GFP-^{S}CwlC indeed still accumulated in one or more distinct rings in cephalexin-treated filaments (Fig. 11D).

We conclude that septal targeting of ^{S}CwlC, ^{S}DamX, and ^{S}DedD is significantly less sensitive to a lack of the essential division activity of FtsN than ^{S}FtsN and ^{S}RlpA. This raises the possibility that the former three recognize a septal target that is distinct from that of the latter two. On the other hand, we note that blocking cell constriction by ^{E}FtsN depletion or cephalexin treatment was not fully effective as judged by the presence of one or more mostly shallow constrictions in the resulting filaments. Therefore, it is also possble that all SPOR domains engage the same septal target but that ^{S}CwlC, ^{S}DamX, and ^{S}DedD have a significantly higher affinity for the target than ^{S}FtsN and ^{S}RlpA. In this case, one has to assume that sufficient ^{E}FtsN and PBP3 activities remained in the filaments to create enough of the target to efficiently attract the high-affinity but not the low-affinity SPORs. Either way, the results illustrate that different SPORs can have distinct properties that may be of physiological relevance.

DISCUSSION

We have shown that the essential function of *E. coli* FtsN in cell division can be performed by a small domain (^{E}FtsN) of at most 35 residues centered about the presumed H2 helix in the periplasmic juxtamembrane region (60), and we have identified the C-terminal SPOR domain (^{S}FtsN) as a strong septal localization determinant. In addition, we showed that three additional SPOR-containing proteins in *E. coli*, DamX, DedD, and RlpA, are also septal ring components and that DamX, and especially DedD, play a demonstrable role in the cell constriction process. We found that the isolated SPOR domains of all four *E. coli* proteins, as well as that of the heterologous *B. subtilis* murein amidase CwlC, accumulate sharply at sites of constriction, indicating this is a common property of such domains. In turn, this predicts that many of the SPOR domain proteins that can be identified in a wide range of bacterial species (20) are targeted to constriction sites as well. As the manuscript was being prepared for publication, this was indeed demonstrated for three additional SPOR-containing proteins from three additional species (45). One of these (CC_2007) is essential for division in *Caulobacter crescentus* and may be functionally equivalent to *E. coli* FtsN, as it shares many of its properties (45).

Our results have interesting implications for the role of FtsN in cell division and the manner by which it joins the division apparatus. The abilities of some of the SPOR-less GFP fusions to accumulate at constriction sites to some degree suggests that, besides ^{S}FtsN, an additional localization determinant(s) resides within the first 90 residues of FtsN (Table 4). However, SPOR-less fusions localized poorly at best, suggesting that any specific interactions between SPOR-less FtsN and SR-associated binding sites are weak or that the number of available sites is limiting.

We further found that the accumulation of ^{S}FtsN in a ring occurs at about the time cells initiate constriction and normally depends on ^{E}FtsN activity, although this dependency could be bypassed in cells producing the FtsA^{E124A} protein. An interesting implication of these results is that FtsN joins the division apparatus in a self-enhancing manner, which is a property that is consistent with a role in triggering the constriction phase of the division process.

Taken together with existing biochemical evidence (44, 46, 55), our results suggest the following order of events at the onset of constriction. (i) Once the SR matures to the point where the murein transpeptidase PBP3 (FtsI) has joined the assembly, the SR is poised to initiate the constriction process. (ii) However, cell constriction requires a sufficient level of ^{E}FtsN activity at the SR, and the majority of FtsN is spread along the membrane prior to synthesis of any septal murein. (iii) Even so, a fraction of the FtsN molecules in the membrane interact with the poised SR structure, likely aided by weak specific interactions between the N-terminal portion of FtsN with other SR components (26), and their associated ^{E}FtsN domains stimulate a small amount of constriction and septal murein synthesis. (iv) This murein is processed by multiple activities, including murein amidases, leading to the generation of a sharply localized and transient form of septal murein that also constitutes a high-affinity binding substrate for ^{S}FtsN. (v) Accumulation of this substrate at the SR recruits additional FtsN molecules from elsewhere in the membrane by binding their ^{S}FtsN moieties. (vi) This, in turn, leads to an increased local concentration of ^{E}FtsN at the SR and an enhanced progression of steps iii to vi, and so on.

To understand why FtsN is normally essential for cell division, it is now pertinent to understand what ^{E}FtsN does. Although a self-enhanced accumulation of FtsN at division sites is consistent with a function in triggering constriction, the cell chaining phenotypes of cells with a partial ^{E}FtsN deficiency imply that ^{E}FtsN function is required to sustain the process as well. It seems unlikely that ^{E}FtsN acts as a structural stabilizer of the SR, as both its small size and its inability to noticeably accumulate at SRs by itself argue against it specifically interacting with multiple SR partners. Thus, even though full-length FtsN may be able to interact with multiple SR partners and this may help to stabilize the SR structure (10, 16, 17, 26, 38), this is probably not the reason why the protein is required for division. It is rather more likely that FtsN is essential because ^{E}FtsN is specifically required to stimulate the constriction process, as suggested in the scheme above. The small size of this domain also argues that its activity is more likely to be allosteric than catalytic, and it is attractive to speculate that an interaction between ^{E}FtsN and another essential SR component generates some signal or state that is required for constriction to start and proceed. One straightforward possibility is that ^{E}FtsN stimulates septal murein synthesis directly, for example, by activating the murein transpeptidase PBP3 (46). However, more circuitous routes are possible. For example, binding of ^{E}FtsN to a periplasmic domain of any of several essential transmembrane SR proteins may generate a stimulatory signal that is first transmitted to the Z ring assembly in the cytoplasm, the constriction of which then secondarily induces septal murein synthesis in the periplasm.

Whatever the mode of action of ^{E}FtsN, it is clear that FtsA^{E124A} can, at least partially, compensate for its absence (5) (Fig. 6). FtsA is an attractive candidate for helping to coordinate septal ring activities in the cytoplasmic and periplasmic compartments during cell envelope invagination, and the mutant FtsA^{E124A} protein in the cytoplasm may inadvertently induce the septal murein synthesis machinery in the periplasm to go ahead, even when ^{E}FtsN is lacking in the latter compartment (5).

What does ^{S}FtsN recognize, and how important is this to the division process? Although alternative mechanisms cannot be excluded, it seems likely that ^{S}FtsN and other SPOR domains are attracted to constriction sites by the local accumulation of some form of murein. As neither GFP-^{S}FtsN (Fig. 4C) nor any of the other four SPOR domains we studied (Fig. 9 to 11) lingered at newly created poles, this material must only be transiently available for binding at the constricting SR. The failure of all five SPOR domains to accumulate at constriction sites in cells lacking the three murein amidases AmiA, -B, and -C (Table 5) correlates well with the biochemical evidence that the periplasmic domain of FtsN (including ^{S}FtsN) bound poorly to sacculi from a similar mutant and that both this domain as well as the isolated SPOR domain of CwlC (^{S}CwlC) still interacted with material that remained upon digestion of murein sacculi with purified amidases (44, 55). The simplest interpretation of these results is that ^{S}FtsN specifically recognizes glycan strands that have been, at least partially, denuded of peptide side chains (presumably both free and cross-linked) by amidase action (55). Such denuded strands are likely subject to (partial) detachment from the sacculus and/or to subsequent processing by lytic transglycosylases, which could be responsible for the transient nature of the SPOR-binding substrate. Another possibility is that SPOR domains recognize a murein geometry that is uniquely present at the SR and inherently transient in normally dividing cells, such as the junction between newly split and as-yet-unsplit septal murein.

In any event, our results suggest that the ability of ^{S}FtsN to recognize its binding substrate contributes to FtsN function by helping to concentrate ^{E}FtsN at the SR as soon as constriction begins and that suboptimal levels of ^{E}FtsN activity at the SR lead to increased constriction periods and cell chaining. Helping to increase ^{E}FtsN activity at the SR may be the only function of the SPOR domain, but it is attractive to speculate on additional roles. For example, FtsN seems well placed to also serve a quality control function during the constriction process. Thus, any problem in septal murein assembly or processing that reduces the availability or accessibility of the ^{S}FtsN substrate might well lead to a reduction in the concentration of ^{E}FtsN at the SR and a commensurate reduction in the constriction rate. The existence and importance of such a function may only become apparent under special circumstances, and further work will be needed to explore this possibility further.

Lastly, the identification of DamX, DedD, and RlpA as new SR components raises the issues of how and when they are recruited to the assembly and, especially, what their roles are. As with FtsN, their SPOR domains are likely dominant septal localization determinants, but additional domains may help recruit each of these proteins to the SR as well. The localization patterns of isolated SPOR domains in ^{E}FtsN-depleted filaments raise the possibility that DamX and DedD localize to division sites prior to RlpA and FtsN itself, but an accurate determination of their time and order of recruitment to the SR will require careful analyses.

Next to Pal, RlpA is now the second outer membrane lipoprotein found to accumulate at constriction sites. As part of the Tol-Pal system, Pal is needed for proper invagination of the OM during cell constriction (24). By connecting the OM with the underlying murein layer via its SPOR domain, RlpA could fulfill a similar function. However, we failed to detect any division defect in Δ*rlpA* mutants (Table 3 and data not shown). Whether RlpA has some redundant role in cell constriction itself or whether its accumulation at division sites is related to some other function remains to be seen. In addition to its septal localization, RlpA-RFP also accumulated into foci (or, possibly, more extended structures) along the cell periphery in both dividing and nondividing cells, suggesting involvement in a nondivision process as well. In this regard it may be relevant that *rlpA* lies in an operon with the genes for the cell shape proteins PBP2 (*mrdA*) and RodA (*mrdB*) (21, 53), although Δ*rlpA* cells showed no obvious shape defect (data not shown).

Whereas the function of RlpA remains unclear, our mutant analyses indicated that DamX and DedD are genuine cell division proteins. Otherwise-wild-type cells lacking DamX showed no obvious phenotype, but absence of the protein aggravated the division defects of *ftsN*^{slm117} or Δ*dedD* cells, suggesting that DamX plays a relatively minor accessory role in the division process that is redundant to that of FtsN and/or DedD.

The role of DedD was more obvious, as cells lacking the protein displayed a distinct chaining phenotype. Moreover, depletion of DedD caused lethal filamentation in *ftsN*^{slm117}

cells, indicating that cells with limited ^{E}FtsN activty come to rely on DedD to accomplish fission. This could mean that DedD is required for full ^{E}FtsN function, or that it can partially subtitute for it, and it will be interesting to elucidate the role of DedD in more detail.

ACKNOWLEDGMENTS

We thank Steven Sandler and Peter Setlow for materials and Andrea Möll, Martin Thanbichler, and David Weiss for communicating results prior to publication.

This work was supported by NIH GM57059 (to P.D.) and NIH NRSA Institutional Training Grant T32GM08056 (to F.B.). Thomas G. Bernhardt holds a Career Award in the Biomedical Sciences from the Burroughs Wellcome Fund.

REFERENCES

1. **Addinall, S. G., C. Cao, and J. Lutkenhaus.** 1997. FtsN, a late recruit to the septum in *Escherichia coli*. Mol. Microbiol. **25:**303–309.
2. **Baba, T., T. Ara, M. Hasegawa, Y. Takai, Y. Okumura, M. Baba, K. A. Datsenko, M. Tomita, B. L. Wanner, and H. Mori.** 2006. Construction of *Escherichia coli* K-12 in-frame, single-gene knockout mutants: the Keio collection. Mol. Syst. Biol. **2:**2006.0008.
3. **Bendezu, F. O., and P. A. de Boer.** 2008. Conditional lethality, division defects, membrane involution, and endocytosis in *mre* and *mrd* shape mutants of *Escherichia coli*. J. Bacteriol. **190:**1792–1811.
4. **Bendezu, F. O., C. A. Hale, T. G. Bernhardt, and P. A. de Boer.** 2009. RodZ (YfgA) is required for proper assembly of the MreB actin cytoskeleton and cell shape in *E. coli*. EMBO J. **28:**193–204.
5. **Bernard, C. S., M. Sadasivam, D. Shiomi, and W. Margolin.** 2007. An altered FtsA can compensate for the loss of essential cell division protein FtsN in *Escherichia coli*. Mol. Microbiol. **64:**1289–1305.
6. **Bernhardt, T. G., and P. A. de Boer.** 2004. Screening for synthetic lethal mutants in *Escherichia coli* and identification of EnvC (YibP) as a periplasmic septal ring factor with murein hydrolase activity. Mol. Microbiol. **52:** 1255–1269.
7. **Bernhardt, T. G., and P. A. de Boer.** 2005. SlmA, a nucleoid-associated, FtsZ binding protein required for blocking septal ring assembly over chromosomes in *E. coli*. Mol. Cell **18:**555–564.
8. **Bernhardt, T. G., and P. A. J. de Boer.** 2003. The *Escherichia coli* amidase AmiC is a periplasmic septal ring component exported via the twin-arginine transport pathway. Mol. Microbiol. **48:**1171–1182.
9. **Chen, J. C., and J. Beckwith.** 2001. FtsQ, FtsL and FtsI require FtsK, but not FtsN, for co-localization with FtsZ during *Escherichia coli* cell division. Mol. Microbiol. **42:**395–413.
10. **Corbin, B. D., B. Geissler, M. Sadasivam, and W. Margolin.** 2004. Z-ring-independent interaction between a subdomain of FtsA and late septation proteins as revealed by a polar recruitment assay. J. Bacteriol. **186:**7736–7744.
11. **Dai, K., Y. Xu, and J. Lutkenhaus.** 1993. Cloning and characterization of *ftsN*, an essential cell division gene in *Escherichia coli* isolated as a multicopy suppressor of *ftsA12*(Ts). J. Bacteriol. **175:**3790–3797.
12. **Dai, K., Y. Xu, and J. Lutkenhaus.** 1996. Topological characterization of the essential *Escherichia coli* cell division protein FtsN. J. Bacteriol. **178:**1328–1334.
13. **Datsenko, K. A., and B. L. Wanner.** 2000. One-step inactivation of chromosomal genes in *Escherichia coli* K-12 using PCR products. Proc. Natl. Acad. Sci. USA **97:**6640–6645.
14. **de Boer, P. A. J., R. E. Crossley, and L. I. Rothfield.** 1989. A division inhibitor and a topological specificity factor coded for by the minicell locus determine proper placement of the division septum in *E. coli*. Cell **56:**641–649.
15. **den Blaauwen, T., M. A. de Pedro, M. Nguyen-Disteche, and J. A. Ayala.** 2008. Morphogenesis of rod-shaped sacculi. FEMS Microbiol. Rev. **32:**321–344.
16. **Derouaux, A., B. Wolf, C. Fraipont, E. Breukink, M. Nguyen-Disteche, and M. Terrak.** 2008. The monofunctional glycosyltransferase of *Escherichia coli* localizes to the cell division site and interacts with penicillin-binding protein 3, FtsW, and FtsN. J. Bacteriol. **190:**1831–1834.
17. **Di Lallo, G., M. Fagioli, D. Barionovi, P. Ghelardini, and L. Paolozzi.** 2003. Use of a two-hybrid assay to study the assembly of a complex multicomponent protein machinery: bacterial septosome differentiation. Microbiology **149:**3353–3359.
18. **Draper, G. C., N. McLennan, K. Begg, M. Masters, and W. D. Donachie.** 1998. Only the N-terminal domain of FtsK functions in cell division. J. Bacteriol. **180:**4621–4627.
19. **Errington, J., R. A. Daniel, and D. J. Scheffers.** 2003. Cytokinesis in bacteria. Microbiol. Mol. Biol. Rev. **67:**52–65.
20. **Finn, R. D., J. Tate, J. Mistry, P. C. Coggill, S. J. Sammut, H. R. Hotz, G. Ceric, K. Forslund, S. R. Eddy, E. L. Sonnhammer, and A. Bateman.** 2008. The Pfam Protein Families Database. Nucleic Acids Res. **36:**D281–D288.
21. **Gama-Castro, S., V. Jimenez-Jacinto, M. Peralta-Gil, A. Santos-Zavaleta, M. I. Penaloza-Spinola, B. Contreras-Moreira, J. Segura-Salazar, L. Muniz-Rascado, I. Martinez-Flores, H. Salgado, C. Bonavides-Martinez, C. Abreu-Goodger, C. Rodriguez-Penagos, J. Miranda-Rios, E. Morett, E. Merino, A. M. Huerta, L. Trevino-Quintanilla, and J. Collado-Vides.** 2008. RegulonDB (version 6.0): gene regulation model of *Escherichia coli* K-12 beyond transcription, active (experimental) annotated promoters and Textpresso navigation. Nucleic Acids Res. **36:**D120–D124.
22. **Geissler, B., and W. Margolin.** 2005. Evidence for functional overlap among multiple bacterial cell division proteins: compensating for the loss of FtsK. Mol. Microbiol. **58:**596–612.
23. **Gerdes, S. Y., M. D. Scholle, J. W. Campbell, G. Balazsi, E. Ravasz, M. D. Daugherty, A. L. Somera, N. C. Kyrpides, I. Anderson, M. S. Gelfand, A. Bhattacharya, V. Kapatral, M. D'Souza, M. V. Baev, Y. Grechkin, F. Mseeh, M. Y. Fonstein, R. Overbeek, A. L. Barabasi, Z. N. Oltvai, and A. L. Osterman.** 2003. Experimental determination and system level analysis of essential genes in *Escherichia coli* MG1655. J. Bacteriol. **185:**5673–5684.
24. **Gerding, M. A., Y. Ogata, N. D. Pecora, H. Niki, and P. A. de Boer.** 2007. The trans-envelope Tol-Pal complex is part of the cell division machinery and required for proper outer-membrane invagination during cell constriction in *E. coli*. Mol. Microbiol. **63:**1008–1025.
25. **Goehring, N. W., and J. Beckwith.** 2005. Diverse paths to midcell: assembly of the bacterial cell division machinery. Curr. Biol. **15:**R514–R526.
26. **Goehring, N. W., C. Robichon, and J. Beckwith.** 2007. Role for the nonessential N terminus of FtsN in divisome assembly. J. Bacteriol. **189:**646–649.
27. **Guyer, M. S., R. R. Reed, J. A. Steitz, and K. B. Low.** 1981. Identification of a sex-factor-affinity site in *E. coli* as gamma delta. Cold Spring Harbor Symp. Quant. Biol. **45:**135–140.
28. **Guzman, L. M., D. Belin, M. J. Carson, and J. Beckwith.** 1995. Tight regulation, modulation, and high-level expression by vectors containing the arabinose P_{BAD} promoter. J. Bacteriol. **177:**4121–4130.
29. **Haldimann, A., and B. L. Wanner.** 2001. Conditional-replication, integration, excision, and retrieval plasmid-host systems for gene structure-function studies of bacteria. J. Bacteriol. **183:**6384–6393.
30. **Hale, C. A., and P. A. J. de Boer.** 1999. Recruitment of ZipA to the septal ring of *Escherichia coli* is dependent on FtsZ and independent of FtsA. J. Bacteriol. **181:**167–176.
31. **Hale, C. A., and P. A. J. de Boer.** 2002. ZipA is required for recruitment of FtsK, FtsQ, FtsL, and FtsN to the septal ring in *Escherichia coli*. J. Bacteriol. **184:**2552–2556.
32. **Hale, C. A., H. Meinhardt, and P. A. J. de Boer.** 2001. Dynamic localization cycle of the cell division regulator MinE in *E. coli*. EMBO J. **20:**1563–1572.
33. **Hamilton, C. M., M. Aldea, B. K. Washburn, P. Babitzke, and S. R. Kushner.** 1989. New method for generating deletions and gene replacements in *Escherichia coli*. J. Bacteriol. **171:**4617–4622.
34. **Heidrich, C., M. F. Templin, A. Ursinus, M. Merdanovic, J. Berger, H. Schwarz, M. A. de Pedro, and J. V. Höltje.** 2001. Involvement of N-acetylmuramyl-L-alanine amidases in cell separation and antibiotic-induced autolysis of *Escherichia coli*. Mol. Microbiol. **41:**167–178.
35. **Johnson, J. E., L. L. Lackner, and P. A. J. de Boer.** 2002. Targeting of ^{D}MinC/MinD and ^{D}MinC/DicB complexes to septal rings in *Escherichia coli* suggests a multistep mechanism for MinC-mediated destruction of nascent FtsZ-rings. J. Bacteriol. **184:**2951–2962.
36. **Johnson, J. E., L. L. Lackner, C. A. Hale, and P. A. De Boer.** 2004. ZipA is required for targeting of ^{D}MinC/DicB, but not ^{D}MinC/MinD, complexes to septal ring assemblies in *Escherichia coli*. J. Bacteriol. **186:**2418–2429.
37. **Jonczyk, P., R. Hines, and D. W. Smith.** 1989. The *Escherichia coli dam* gene is expressed as a distal gene of a new operon. Mol. Gen. Genet. **217:**85–96.
38. **Karimova, G., N. Dautin, and D. Ladant.** 2005. Interaction network among *Escherichia coli* membrane proteins involved in cell division as revealed by bacterial two-hybrid. analysis. J. Bacteriol. **187:**2233–2243.
39. **Kuroda, A., Y. Asami, and J. Sekiguchi.** 1993. Molecular cloning of a sporulation-specific cell wall hydrolase gene of *Bacillus subtilis*. J. Bacteriol. **175:** 6260–6268.
40. **Lackner, L. L., D. M. Raskin, and P. A. de Boer.** 2003. ATP-dependent interactions between *Escherichia coli* Min proteins and the phospholipid membrane in vitro. J. Bacteriol. **185:**735–749.
41. **Lewis, K.** 2000. Programmed death in bacteria. Microbiol. Mol. Biol. Rev. **64:**503–514.
42. **Lobner-Olesen, A., E. Boye, and M. G. Marinus.** 1992. Expression of the *Escherichia coli dam* gene. Mol. Microbiol. **6:**1841–1851.
43. **Lyngstadaas, A., A. Lobner-Olesen, and E. Boye.** 1995. Characterization of three genes in the dam-containing operon of *Escherichia coli*. Mol. Gen. Genet. **247:**546–554.
44. **Mishima, M., T. Shida, K. Yabuki, K. Kato, J. Sekiguchi, and C. Kojima.** 2005. Solution structure of the peptidoglycan binding domain of *Bacillus subtilis* cell wall lytic enzyme CwlC: characterization of the sporulation-related repeats by NMR. Biochemistry **44:**10153–10163.
45. **Moll, A., and M. Thanbichler.** 2009. FtsN-like proteins are conserved com-

ponents of the cell division machinery in proteobacteria. Mol. Microbiol. **72:**1037–1053.
46. **Muller, P., C. Ewers, U. Bertsche, M. Anstett, T. Kallis, E. Breukink, C. Fraipont, M. Terrak, M. Nguyen-Disteche, and W. Vollmer.** 2007. The essential cell division protein FtsN interacts with the murein (peptidoglycan) synthase PBP1B in *Escherichia coli*. J. Biol. Chem. **282:**36394–36402.
47. **Nonet, M. L., C. C. Marvel, and D. R. Tolan.** 1987. The hisT-purF region of the *Escherichia coli* K-12 chromosome. Identification of additional genes of the hisT and purF operons. J. Biol. Chem. **262:**12209–12217.
48. **Reddy, M.** 2007. Role of FtsEX in cell division of *Escherichia coli*: viability of *ftsEX* mutants is dependent on functional SufI or high osmotic strength. J. Bacteriol. **189:**98–108.
49. **Rodolakis, A., P. Thomas, and J. Starka.** 1973. Morphological mutants of *Escherichia coli*. Isolation and ultrastructure of a chain-forming envC mutant. J. Gen. Microbiol. **75:**409–416.
50. **Santini, C. L., A. Bernadac, M. Zhang, A. Chanal, B. Ize, C. Blanco, and L. F. Wu.** 2001. Translocation of jellyfish green fluorescent protein via the Tat system of *Escherichia coli* and change of its periplasmic localization in response to osmotic up-shock. J. Biol. Chem. **276:**8159–8164.
51. **Shida, T., H. Hattori, F. Ise, and J. Sekiguchi.** 2001. Mutational analysis of catalytic sites of the cell wall lytic N-acetylmuramoyl-L-alanine amidases CwlC and CwlV. J. Biol. Chem. **276:**28140–28146.
52. **Smith, T. J., and S. J. Foster.** 1995. Characterization of the involvement of two compensatory autolysins in mother cell lysis during sporulation of *Bacillus subtilis* 168. J. Bacteriol. **177:**3855–3862.
53. **Takase, I., F. Ishino, M. Wachi, H. Kamata, M. Doi, S. Asoh, H. Matsuzawa, T. Ohta, and M. Matsuhashi.** 1987. Genes encoding two lipoproteins in the leuS-dacA region of the *Escherichia coli* chromosome. J. Bacteriol. **169:** 5692–5699.
54. **Thomas, J. D., R. A. Daniel, J. Errington, and C. Robinson.** 2001. Export of active green fluorescent protein to the periplasm by the twin-arginine translocase (Tat) pathway in *Escherichia coli*. Mol. Microbiol. **39:**47–53.
55. **Ursinus, A., F. van den Ent, S. Brechtel, M. de Pedro, J. V. Holtje, J. Lowe, and W. Vollmer.** 2004. Murein (peptidoglycan) binding property of the essential cell division protein FtsN from *Escherichia coli*. J. Bacteriol. **186:** 6728–6737.
56. **Vollmer, W., and U. Bertsche.** 2008. Murein (peptidoglycan) structure, architecture and biosynthesis in *Escherichia coli*. Biochim. Biophys. Acta **1778:** 1714–1734.
57. **Wang, L., M. K. Khattar, W. D. Donachie, and J. Lutkenhaus.** 1998. FtsI and FtsW are localized to the septum in *Escherichia coli*. J. Bacteriol. **180:**2810–2816.
58. **Wang, X., P. A. J. de Boer, and L. I. Rothfield.** 1991. A factor that positively regulates cell division by activating transcription of the major cluster of essential cell division genes of *Escherichia coli*. EMBO J. **10:**3363–3372.
59. **Wissel, M. C., and D. S. Weiss.** 2004. Genetic analysis of the cell division protein FtsI (PBP3): amino acid substitutions that impair septal localization of FtsI and recruitment of FtsN. J. Bacteriol. **186:**490–502.
60. **Yang, J. C., F. Van Den Ent, D. Neuhaus, J. Brevier, and J. Lowe.** 2004. Solution structure and domain architecture of the divisome protein FtsN. Mol. Microbiol. **52:**651–660.
61. **Yu, D., H. M. Ellis, E. C. Lee, N. A. Jenkins, N. G. Copeland, and D. L. Court.** 2000. An efficient recombination system for chromosome engineering in *Escherichia coli*. Proc. Natl. Acad. Sci. USA **97:**5978–5983.